ELEMENTA
Science of the Anthropocene

Seasonal sea ice changes in the Amundsen Sea, Antarctica, over the period of 1979–2014

S. E. Stammerjohn[1*] • T. Maksym[2] • R. A. Massom[3,4] • K. E. Lowry[5] • K. R. Arrigo[5] • X. Yuan[6] • M. Raphael[7] • E. Randall-Goodwin[8] • R. M. Sherrell[9] • P. L. Yager[10]

[1]Institute of Arctic and Alpine Research, University of Colorado, Boulder, Colorado, United States
[2]Woods Hole Oceanographic Institution, Woods Hole, Massachusetts, United States
[3]Australian Antarctic Division, Kingston, Tasmania, Australia
[4]Antarctic Climate and Ecosystems Cooperative Research Centre, University of Tasmania, Hobart, Tasmania, Australia
[5]Department of Environmental Earth System Science, Stanford University, Stanford, California, United States
[6]Lamont-Doherty Earth Observatory, Columbia University, New York, United States
[7]Department of Geography, University of California, Los Angeles, California, United States
[8]Scripps Institution of Oceanography, University of California, San Diego, California, United States
[9]Department of Marine and Coastal Sciences and Department of Earth and Planetary Sciences, Rutgers University, New Brunswick, New Jersey, United States
[10]Department of Marine Sciences, University of Georgia, Athens, Georgia, United States

*sharon.stammerjohn@colorado.edu

Abstract

Recent attention has focused on accelerated glacial losses along the Amundsen Sea coast that result from changes in atmosphere and ocean circulation, with sea ice playing a mediating but not well-understood role. Here, we investigated how sea ice has changed in the Amundsen Sea over the period of 1979 to 2014, focusing on spatio-temporal changes in ice edge advance/retreat and percent sea ice cover in relation to changes in winds. In contrast to the widespread sea ice decreases to the east and increases to the west of the Amundsen Sea, sea ice changes in the Amundsen Sea were confined to three areas: (i) offshore of the shelf break, (ii) the southern Pine Island Polynya, and (iii) the eastern Amundsen Sea Polynya. Offshore, a 2-month decrease in ice season duration coincided with seasonal shifts in wind speed and direction from March to May (relating to later ice advance) and from September to August (relating to earlier retreat), consistent with reported changes in the depth/location of the Amundsen Sea Low. In contrast, sea ice decreases in the polynya areas corresponded to episodic or step changes in spring ice retreat (earlier by 1–2 months) and were coincident with changes to Thwaites Iceberg Tongue (located between the two polynyas) and increased southeasterly winds. Temporal correlations among these three areas were weak, indicating different local forcing and/or differential response to large-scale forcing. Although our analysis has shown that part of the variability can be explained by changes in winds or to the coastal icescape, an additional but unknown factor is how sea ice has responded to changes in ocean heat and freshwater inputs. Unraveling cause and effect, critical for predicting changes to this rapidly evolving ocean-ice shelf-sea ice system, will require in situ observations, along with improved remote sensing capabilities and ocean modeling.

Domain Editor-in-Chief
Jody W. Deming, University of Washington

Associate Editor
Edward C. Carmack, Fisheries & Oceans Canada

Knowledge Domain
Ocean Science

Article Type
Research Article

Part of an *Elementa* Special Feature
ASPIRE: The Amundsen Sea Polynya International Research Expedition

Received: October 6, 2014
Accepted: May 20, 2015
Published: June 30, 2015

Introduction

The Amundsen Sea embayment (Figure 1) is a current hot spot of rapidly thinning ice shelves, high calving fluxes, and rapidly retreating marine-grounded glaciers (Pritchard et al., 2012; Rignot et al., 2014). Estimates of basal ice shelf melt and calving flux are some of the highest observed anywhere in coastal Antarctica (Rignot et al., 2013; Paolo et al., 2015). In contrast, the adjacent sea ice cover to the north is legendary for thwarting early exploration of the continental shelf region due to some of the thickest, most persistent, and most heavily snow-laden sea ice observed anywhere in the Antarctic (Jacobs et al., 2012; Xie et al., 2013; Kwok and Maksym, 2014). Only since the 1990s have ice-strengthened vessels been able to explore the continental

shelf and coastal region, with navigation likely made possible by several years of decreased summer sea ice in the late 1980s and early 1990s (Jacobs and Comiso, 1993, 1997).

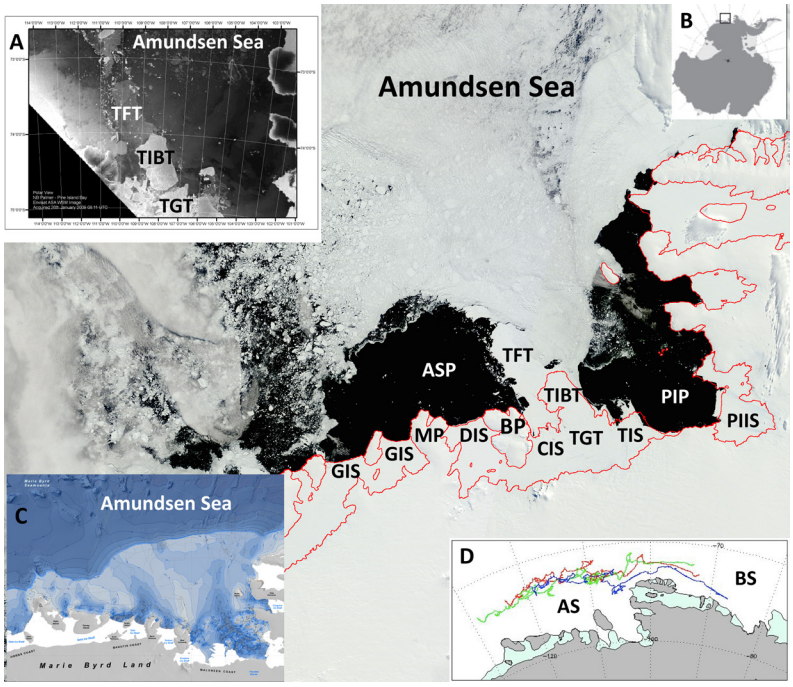

Figure 1

Amundsen Sea study region.

MODIS Terra image (at 250 m resolution) acquired on 2 January 2011 showing early-summer sea ice coverage in the Amundsen Sea region and open water extents in the two coastal polynyas. Place names are, from east to west: Pine Island Ice Shelf (PIIS), Pine Island Polynya (PIP), Thwaites (eastern) Ice Shelf (TIS), Thwaites Glacier Tongue (TGT), Thwaites Iceberg Tongue (TIBT), Thwaites Fast-ice Tongue (TFT), Crosson Ice Shelf (CIS), Bear Peninsula (BP), Dotson Ice Shelf (DIS), Amundsen Sea Polynya (ASP), Martin Peninsula (MP), and Getz Ice Shelf (GIS). The coastline (in red) is from MOA 2009 (Haran et al., 2014). (A) European Space Agency Envisat SAR image from 26 January 2009 revealing details of the TGT, TIBT and TFT. The relatively smooth surface of the fast ice appears dark relative to the rougher surface of the small icebergs within and bordering the TFT, and relative to the rougher surfaces of the TGT and TIBT. (B) Location map. (C) Bathymetry of the Amundsen Sea continental shelf region (blue-gray shading at 100-m depth intervals) (Nitsche et al., 2007). (D) The westward drift tracks of three ice buoys deployed in the Bellingshausen Sea (BS) in March 2007; drift ended in the Amundsen Sea (AS).

doi: 10.12952/journal.elementa.000055.f001

The Amundsen Sea sits between two regions showing large but opposing sea ice extent and concentration trends, as observed since 1979 (e.g., Yuan and Martinson, 2000; Turner et al., 2009; Stammerjohn et al., 2012; Simpkins et al., 2013). To the east in the Bellingshausen Sea, the sea ice season is on average three months shorter, while to the west in the western Ross Sea (Figure 2B) it is on average two months longer (Stammerjohn et al., 2012). In contrast, sea ice changes in the Amundsen Sea are more localized (Figure 2), interspersed between areas showing relatively high yearly variability (Simpkins et al., 2012).

Some of the first sea ice studies to draw attention to the Amundsen Sea were those documenting the large decreases in summer sea ice in the southern Bellingshausen and eastern Amundsen Sea region in the late 1980s and early 1990s (Jacobs and Comiso, 1993, 1997). It was noted then that much of the multi-year sea ice was removed from the continental shelf areas during the extreme summer minima between 1987 and 1994, with likely impacts on regional mean sea ice thickness, vertical heat flux, ice formation and brine production. The several-year sea ice decreases also suggested links to large-scale circulation changes in the South Pacific, including changes affecting winds, surface ocean currents, and upwelling of warm Circumpolar Deep Water (CDW) on the continental shelf (Jacobs and Comiso, 1997).

Sea ice variability in the West Antarctic sector of the Southern Ocean is largely wind-driven (Assmann et al., 2005; Massom et al., 2008; Holland and Kwok, 2012), particularly in spring, with possible ocean feedbacks contributing to autumn sea ice changes (Nihashi and Ohshima, 2001; Stammerjohn et al., 2012; Holland, 2014). Sea ice can also mediate ocean-ice shelf interactions through its effect on ocean stratification and dampening of wind stress (e.g., Dinniman et al., 2012; Petty et al., 2014). In turn, changes in air-ocean interactions and heat and freshwater inputs affect sea ice distributions and rates of growth and melt (Assmann et al., 2005). The heat and freshwater inputs can be from upwelled CDW exiting the ice shelf cavities made buoyant from basal ice shelf melt but still up to a few degrees above freezing (Jacobs et al., 2012) and/or from solar-heated waters and net sea ice or surface glacial melt.

Ocean circulation is affected by wind, and an increase in westerly winds over the Amundsen Sea region (Bracegirdle, 2013) has been associated with increases in warm CDW flowing onto the continental shelf (Thoma et al., 2008; Arneborg et al., 2012; Wåhlin et al., 2012; Assmann et al., 2013; Walker et al., 2013). Once on the shelf, the warm CDW flows towards the coast along down-sloping troughs bisecting the continental shelf (Nitsche et al., 2007) to circulate under the floating ice shelves, causing basal ice shelf melt (Jenkins et al., 2010; Jacobs et al., 2011; Dutrieux et al., 2014).

Air-ocean-ice interactions in the Amundsen Sea region are thought to be sensitive to large-scale climate variability and tropical teleconnections; e.g., the Southern Annular Mode (SAM) (e.g., Turner et al., 2009), El Niño-Southern Oscillation (ENSO) (e.g., Yuan, 2004), the Atlantic Multi-decadal Oscillation (Li et al., 2014; Simpkins et al., 2014), and warming in the central tropical Pacific (Steig et al., 2012). However, the sensitivity of sea ice in the Amundsen Sea to large-scale climate variability will likely vary between the

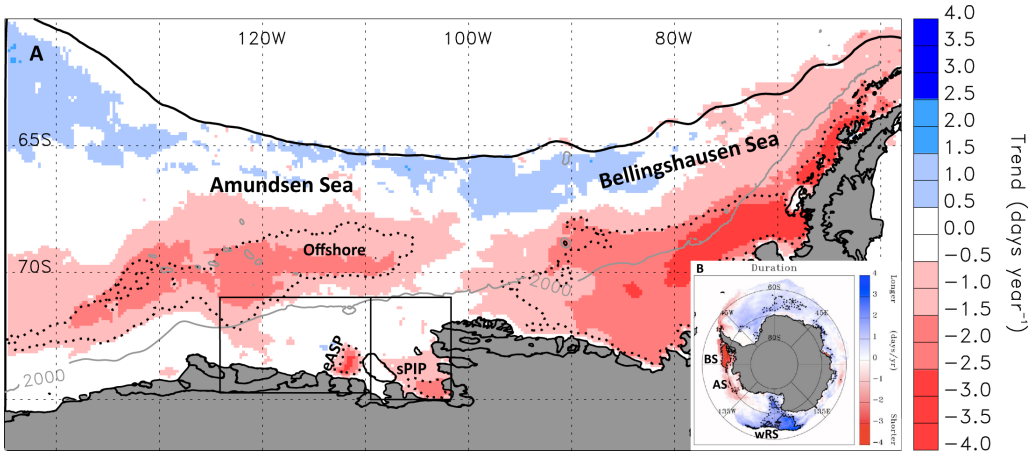

Figure 2

Trends in annual ice season duration in the Amundsen Sea.

(A) Map of annual ice season duration trend (days year^{-1}) for the period of 1979/80 to 2013/14 in the Bellingshausen-Amundsen Sea, showing strong negative trends (shorter sea ice season) in most areas (updated from Stammerjohn et al., 2012). The upper black solid contour outlines the mean max winter sea ice extent. The black dotted contour outlines those areas where the trend is significant at the $p < 0.01$ level based on the assumption that the time series at each pixel is Gaussian distributed and stationary (an assumption that is violated in the two coastal areas, as further explored in Figures 8 and 11). The gray solid contour outlines the 2000-m isobath, approximating the continental shelf slope location. The boxed areas adjacent to the Amundsen coast enclose the mean maximum extents of the Pine Island and Amundsen Sea polynyas. Labeled areas include the Offshore, the southern Pine Island Polynya (sPIP) and the eastern Amundsen Sea Polynya (eASP), each delimited by the black dotted contour, and for the Offshore area, includes the dotted area between 105–125°W. (B) Map of sea ice duration trends for the entire Southern Ocean, showing the locations of the Bellingshausen Sea (BS), Amundsen Sea (AS) and the western Ross Sea (wRS).

doi: 10.12952/journal.elementa.000055.f002

exposed offshore region and the partially enclosed coastal area. Thus, trying to unravel the source of sea ice variability in the Amundsen Sea is challenging given the juxtaposition of both local and large-scale influences.

Prominent features of the Amundsen Sea coastal area are its polynyas, the two largest being the highly variable Pine Island Polynya (PIP) and the Amundsen Sea Polynya (ASP) (Figure 1). On average, the PIP begins to increase in size in November and then rapidly decreases in March. The ASP opens and closes with timing similar to the PIP, though it is considerably less variable (Arrigo et al., 2012). These two polynyas are separated by a shoal (< 300 m) extending northwards from Bear Peninsula (e.g., Nitsche et al., 2007). Over the top of this shallow ridge is a spatially variable tongue of thick fast ice, and to its south, the Thwaites Iceberg Tongue. Both features extend roughly northwards from the Thwaites Glacier Tongue (Figure 1) (e.g., Ferrigno et al., 1993; MacGregor et al., 2012).

The Thwaites Iceberg Tongue is composed mostly of larger icebergs, including typically a very large tabular iceberg (~ 40–50 km wide and ~ 80 km long), whereas the fast-ice tongue to its north is anchored on its western side by numerous relatively small, grounded icebergs (Figure 1A). Together, the Thwaites Fast-ice and Iceberg Tongue (TFIT) present a formidable barrier to sea ice circulation in the southeast sector of the Amundsen Sea. However, over at least the last 70 years, the extent and composition of the TFIT barrier has varied distinctly (Ferrigno et al., 1993; MacGregor et al., 2012) and has affected sea ice variability in the PIP and ASP as well. In addition, smaller icebergs regularly calve from the TFIT as well as from the glacier tongue. Those that do not ground along the TFIT typically drift northwestward, with some grounding on the outer continental shelf (Figure 1A) to potentially play a role in trapping and retaining summer sea ice to the north of the ASP and PIP areas.

Because of the TFIT barrier, the annually-recurrent ASP is characterized as a barrier coastal polynya, similar to the Mertz Glacier Polynya (Massom et al., 2001) and other coastal polynyas with a glacier tongue, iceberg or fast-ice barriers to their east (Fraser et al., 2012; Nihashi and Ohshima, 2015). Prevailing southeasterly coastal winds blowing over the TFIT keep the ASP ice-free, while the TFIT barrier also prevents sea ice from drifting out of the PIP area into the ASP area.

In summary, the Amundsen Sea presents a conundrum of sea ice variability and change, given its sensitivity to large-scale climate variability and changing coastal icescapes. Identifying the factors contributing to the different sea ice changes is challenging but critical for predicting future change in the coupled cryosphere-ocean-atmosphere system. The impacts of rapid sea ice changes on the marine environment, especially in polynyas, are likewise significant and were key topics explored during the Amundsen Sea Polynya International Research Expedition (ASPIRE) (Yager et al., 2012), the results of which are presented in this Special Feature.

In this study, given the absence of in situ time-series data to investigate changes in ice-ocean interactions in the Amundsen Sea region, we have taken the necessary first step and used the available satellite observations and numerical analyses to assess ice-atmosphere interactions over the period of 1979 to 2014. The approach taken was first to identify where and how sea ice had changed over this period and then to examine relationships between sea ice variability and winds. The results are discussed within the context of regional atmospheric, oceanic and coastal icescape variability. They highlight the critical need for continued and coordinated in situ, satellite and model investigations, if we wish to better understand this highly sensitive and rapidly changing ocean-sea ice-ice shelf system.

Methods

We used satellite-derived and numerically-analyzed surface and atmospheric variables to assess ice-atmosphere interactions in the Amundsen Sea region. These included daily and monthly sea ice concentration and surface

winds. Sea ice concentrations over the period of 1979 to 2012 are from Version 2 of the Goddard Space Flight Center (GSFC) Bootstrap Scanning Multi-channel Microwave Radiometer-Special Sensor Microwave/Imager (SMMR-SSM/I) daily and monthly time series (Comiso, 2000; Comiso and Nishio, 2008; Comiso, 2010), augmented with Near Real-Time Sea Ice daily data after 2012 (Maslanik and Stroeve, 1999) to produce a time series extending from 1979 to 2014. These data were provided by the EOS Distributed Active Archive Center (DAAC) at the National Snow and Ice Data Center (NSIDC, University of Colorado at Boulder, http://nsidc.org).

Using daily sea ice concentrations and following Stammerjohn et al. (2008), we identified the day of annual ice edge advance and retreat for each gridded (25 × 25 km pixel) location and for each sea ice year that begins/ends during the mean summer sea ice minimum (mid-February) to present a time series of sea ice advance and retreat over the period of 1979/80 to 2013/14. We also analyzed winter ice season duration (the time elapsed between the autumn advance and its subsequent spring retreat) and summer open water duration (the time between the spring retreat and its subsequent autumn advance). Finally, we analyzed changes in initial polynya opening, the location of that opening, and its size in spring–summer. Note that when we refer to sea ice change in the polynyas, we are referring to changes in the sea ice cover bordering the polynyas, changes that would affect the polynya opening or its size and duration during summer. During winter, small but variable areas of open water likely persist in both polynyas (Arrigo et al., 2012; Mankoff et al., 2012), but these changes are not well resolved by the coarse-resolution passive microwave satellite data analyzed here.

There are different biases in the satellite-derived sea ice concentrations depending on the algorithm used; e.g., NASA Team versus Bootstrap Version 1 or 2 (Comiso et al., 1997; Eisenman et al., 2014). Although we qualitatively discuss changes in sea ice concentration (e.g., with respect to winds), we only quantified change based on ice edge (e.g., ice edge advance or retreat and the resulting ice season duration) and not on sea ice concentration changes. Estimates of ice edge location have much higher precision than estimates of sea ice concentration due to the large contrast in emissivity between ice and ocean, thus resulting in much smaller differences between algorithms (Steffen et al., 1992; Comiso et al., 1997). For example, variability and trends in ice season duration (an ice edge metric) as estimated by the NASA Team algorithm (Parkinson, 2004) and by the Bootstrap Version 2 algorithm (Stammerjohn et al., 2008) are nearly identical.

Numerically analyzed 10-m winds from the European Centre for Medium Range Weather Forecasts (ECMWF) Interim Reanalysis (ERA-I) (Dee et al., 2011) were used to describe monthly to seasonal changes in wind direction and magnitude. We used data over the period of 1979 to 2013, which includes data quality improvements following incorporation of satellite data into the numerical data analysis in late 1978. Unfortunately, few meteorological data are available for the Amundsen Sea region to help constrain the reanalysis data. However, comparisons with sea-level pressure data from drifting ice buoys in the Bellingshausen Sea showed ERA-I to be the most accurate in capturing individual weather systems (as compared to other reanalysis products), inferring that ERA-I better captures wind variability in the Amundsen Sea as well (Bracegirdle, 2013).

Where appropriate, the temporal changes in the environmental variables (sea ice, winds) were assessed through linear regression. Because these time series contain some degree of autocorrelation, the standard error and significance level of linear trends are based on the effective degrees of freedom present in the regression residuals (following Santer et al., 2000). However, some of the locally derived sea ice time series show episodic or distinct step changes; in those cases, shifts in means are highlighted instead. Correlations between time series are reported for de-trended time series (where necessary), with significance determined using t-test statistics.

Results

In the Amundsen Sea region, three locations exhibited notable ice season decreases over the period of 1979/80 to 2013/14: (i) offshore of the shelf break, (ii) in southern Pine Island Polynya (sPIP), and (iii) in the eastern Amundsen Sea Polynya (eASP) (Figure 2). There was very little covariability among the time series of ice season duration from these three areas (R values of 0.04 to 0.31 between de-trended time series). Further, covariability was weak between the Amundsen Sea offshore area and the high trending areas to both the east, in the southern Bellingshausen Sea, and west, in the western Ross Sea (R values < ± 0.26). Below, we present a detailed analysis of the seasonal sea ice changes in each of these three Amundsen Sea areas, together with observed changes in sea ice concentration and winds. This analysis gives insight into the temporal nature of sea ice change in these three areas, and the degree to which such change can be associated with change in atmospheric circulation.

The offshore area

The offshore area (as defined in Figure 2) straddles latitudes 69–70°S between longitudes 105–125°W and lies mostly north of the continental shelf break. Here, the ice season has shortened on average by 57 days over the period of 1979/80 to 2013/14 due to a later autumn advance (by 34 days) and earlier spring retreat (by 23 days) in sea ice (Figure 3, Table 1). Changes in the autumn sea ice advance are notably larger than

those in the spring retreat and explain a larger fraction of the variability in ice season duration (R = –0.79 versus 0.44, respectively). There was also a slight reprieve in the shortening of the sea ice season during the mid-to-late 1990s.

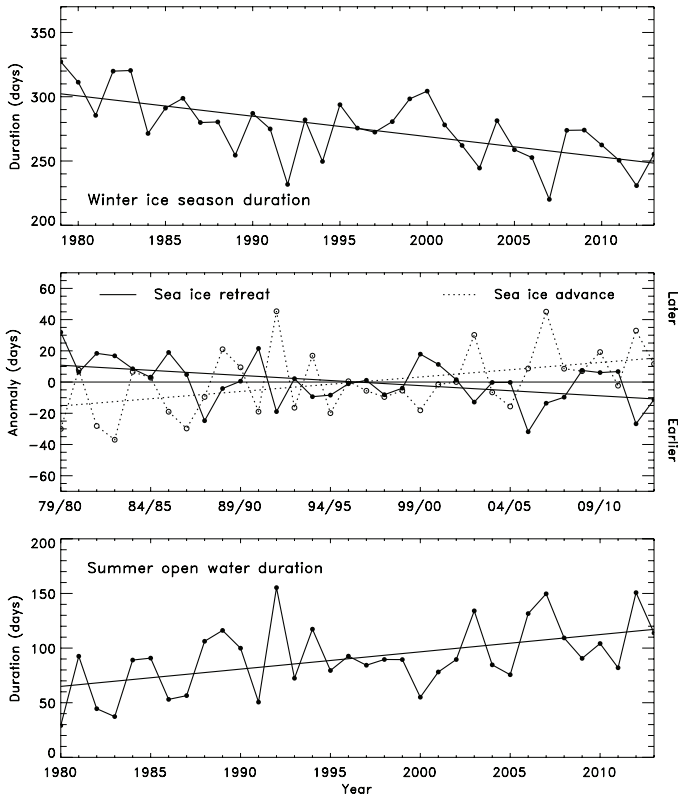

Figure 3

Ice season variability and trends in the offshore region.

Time series and trends in the Offshore Region over the period of 1979/80 to 2013/14 for: (A) sea ice season duration, (B) anomalies in the timing of sea ice retreat and subsequent advance (i.e., the time series for sea ice advance is lagged by 1 year such that the austral spring–summer 1979/80 sea ice retreat is plotted against the subsequent austral autumn 1980 advance), and (C) open water duration. In (B), the temporal correlation between the de-trended time series of sea ice retreat and subsequent advance is –0.54. Statistics are reported in Table 1.

doi: 10.12952/journal.elementa.000055.f003

Table 1. Area-averaged means[a] in day of sea ice advance and retreat, ice season duration, and open water duration over the period of 1979/80 to 2013/14 (and as otherwise noted) for three Amundsen Sea regions; trends[b] are also reported for the offshore region

Region	Metric	Day of advance	Day of retreat	Ice season duration	Open water duration
Offshore	Mean	99	374	275	89
	Trend	1.0 ± 0.4	–0.6 ± 0.3	–1.6 ± 0.4	1.6 ± 0.6
sPIP	Mean	57	389	333	32
	1979–1994	52	403	353	13
	1995–2013	62	376	316	48
eASP	Mean	58	371	314	50
	1979–1992	55	398	344	21
	1993–2013	60	353	294	69

[a]Means are reported in year day for sea ice advance and retreat and in days for ice season duration and open water duration.
[b]Trends are reported in days per year, with standard error and significance determined using the effective degrees of freedom present in the regression residuals (Santer et al., 2000); only those trends with a significance of $p < 0.01$ are reported. Positive trends in advance and open water duration indicate trends towards later advance and longer open water season, respectively; negative trends in retreat and ice season duration indicate trends towards earlier retreat and shorter ice season, respectively.

doi:10.12952/journal.elementa.000055.t001

The offshore area lies in a transition zone between belts of strong northwesterly winds to the north and southeasterly winds to the south (Figures 4 and 5). This area also corresponds to a transition zone in mean wind-driven sea ice motion (not shown), whereby the northwesterly winds to the north tend to drive sea ice eastward through Ekman transport, while to the south southeasterly winds drive the sea ice westwards (see also Assmann et al., 2005). A notable temporal shift in seasonal peak winds occurred from March and September earlier in the record (1979–1995) to May and August later in the record (1996–2013) (Figure 6A). This shift resulted in decreased westerly winds in both March and September over 1979–2013, and both months showed similar decreases in magnitude (–0.06 m s^{-1} yr^{-1}, $p < 0.1$). There also was a strengthening of northerly winds in September and November, with both showing similar increases in magnitude (0.04 m s^{-1} yr^{-1}, $p < 0.1$) (Figure 6B).

The observed seasonal changes in sea ice are consistent with the seasonal changes in peak winds. To illustrate this consistency, examples of wind and sea ice anomalies are shown for late versus early sea ice retreat for three different years for the month of December, the month before the mean day of retreat (Figure 7 A, C, E). In the example of a late spring retreat, northwesterly winds were associated with increases in sea ice concentration and thus slower (later) melt-back (Figure 7A). These increases were due to strong northwesterly winds driving sea ice into the offshore region from the west throughout late winter and early spring. In contrast, an earlier spring retreat occurred when there were decreased sea ice concentrations and either southerly winds driving sea ice northward into solar-heated waters (Figure 7C) or northerly winds driving ice southward (Figure 7E). The decreased sea ice concentrations were due to weakened westerly winds driving less sea ice into the offshore region.

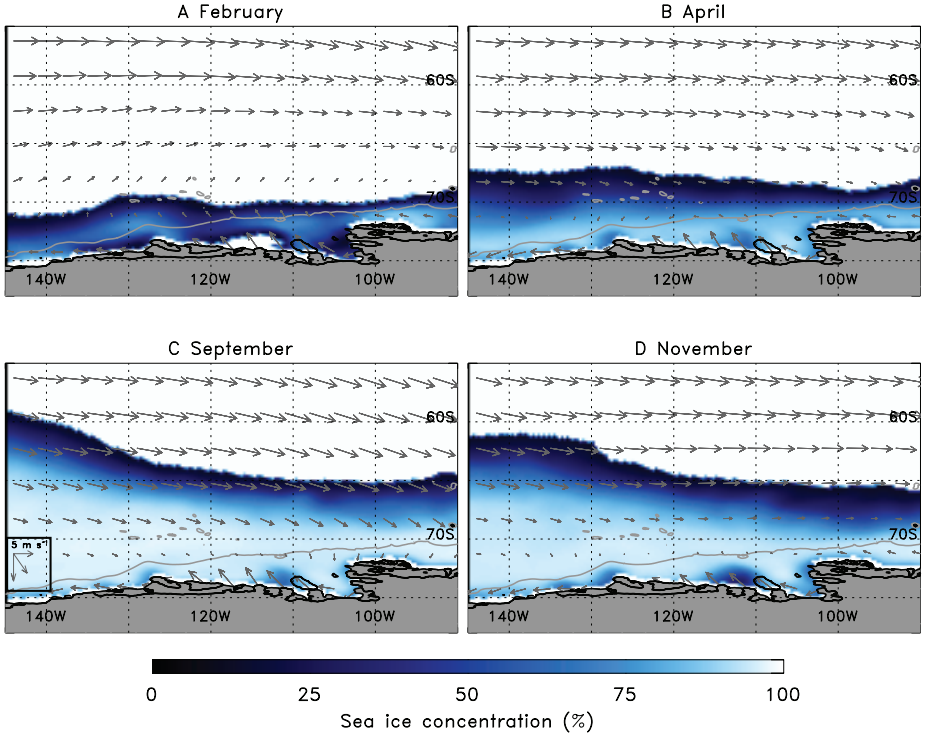

Figure 4

Mean seasonal changes in sea ice concentration and extent.

Mean monthly (1979–2012) sea ice concentration (shading) and winds (arrows) for (A) February, (B) April, (C) September, and (D) November. The gray contour outlines the 2000-m isobath. A legend for the wind speed is given in the lower left corner of (C).

doi: 10.12952/journal.elementa.000055.f004

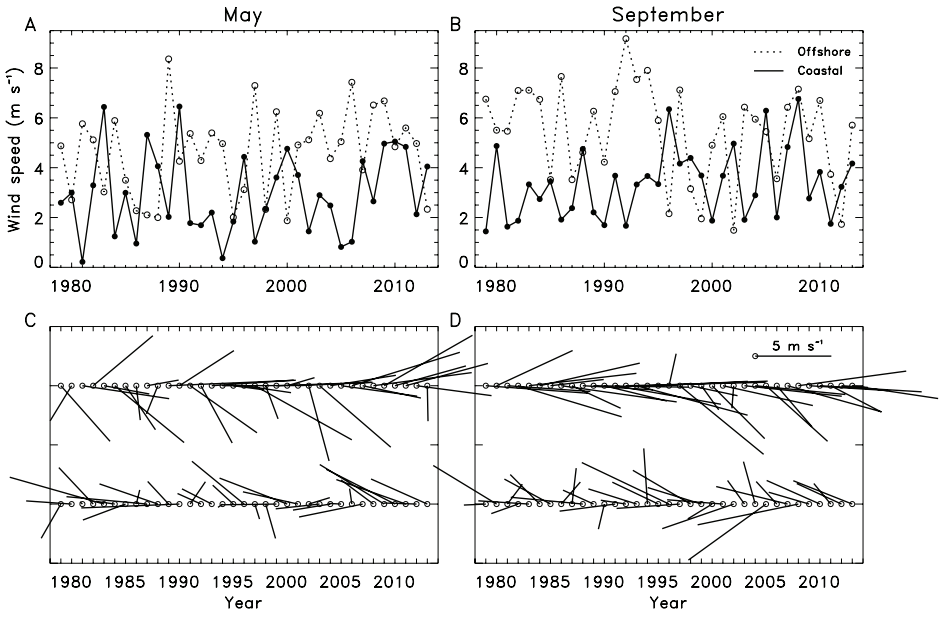

Figure 5

Winds in the offshore versus coastal region.

Time series of (A) May and (B) September monthly mean wind speed over the offshore (dotted) and coastal area (solid), and of (C) May and (D) September monthly mean wind speed and direction, over the offshore (top row of C, D) and coastal (bottom row of C, D) areas. The offshore area extends from 63.75°S to 67.5°S and from 116.25°W to 130.5°W. The coastal area extends from 71.25°S to 75.0°S and from 100.5°W to 120.0°W.

doi: 10.12952/journal.elementa.000055.f005

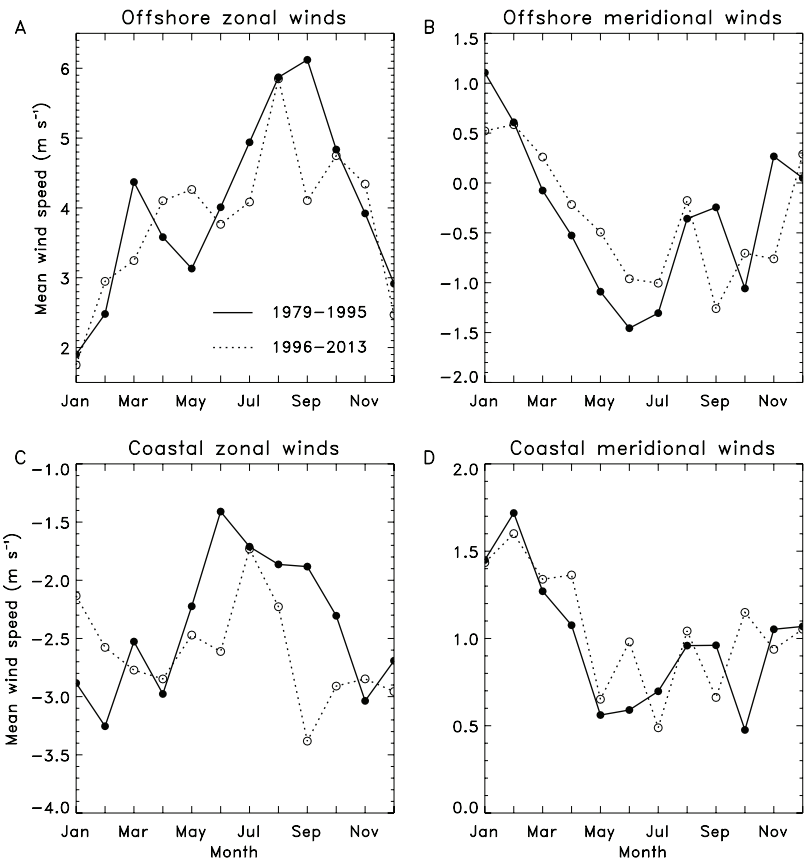

Figure 6

Decadal changes in the offshore and coastal winds.

Mean monthly zonal (A, C) and meridional (B, D) winds for an area north of the offshore (A, B) and coastal (C, D) area, respectively, for 1979–1995 (solid lines) and for 1996–2013 (dotted lines). The offshore and coastal areas are as defined in Figure 5. Positive zonal winds (in A, C) indicate winds from the west, and positive meridional winds (in B, D) indicate winds from the south.

doi: 10.12952/journal.elementa.000055.f006

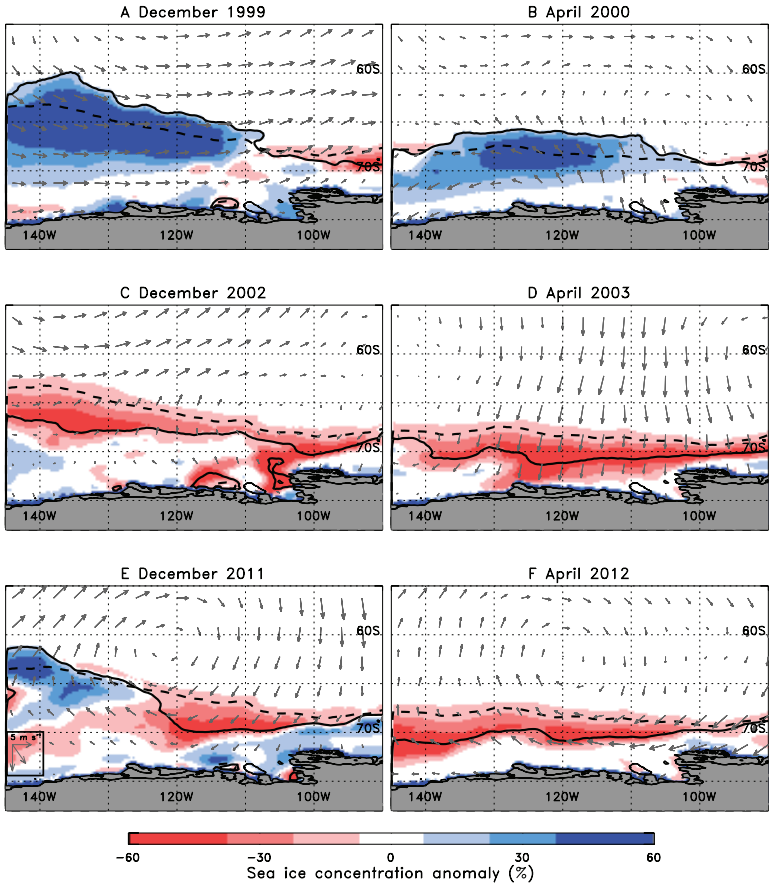

Figure 7

Anomalies in sea ice concentration and winds relevant to the offshore region.

Monthly anomalies in sea ice concentration (shading) and winds (arrows) for December (A, C, E) and April (B, D, F), showing examples of conditions leading to (A, B) a late retreat and early advance, and (C, D and E, F) an early retreat and late advance over the offshore region. The solid and dotted contours delineate the observed and 35-year mean ice edge locations, respectively (based on 15% ice concentration). Mean day of retreat over the offshore region is January 10, as compared to (A) January 29 in 1999, (C) December 28 in 2002, and (E) December 14 in 2011. Mean day of advance over the offshore region is April 8, as compared to (B) March 21 in 2000, (D) May 10 in 2003, and (F) May 11 in 2012. A legend for the wind speed is given in the lower left corner of (E).

doi: 10.12952/journal.elementa.000055.f007

Based on these examples and our analysis of the entire times series, it appears that the observed pronounced decrease in September westerly winds (Figure 6A) contributed to less sea ice being imported from the west into the offshore region. This reduced import coincided with observed decreases in springtime sea ice concentration. Consequently, the ice edge became more vulnerable to early melt-back and retreat with any anomalous increase in meridional winds. In particular, the subsequent increase in northerly winds in November over the period of 1979–2013 (Figure 6B) was another factor contributing to the observed trend towards earlier ice edge retreat (Figures 3B).

Anomalies in wind and sea ice concentration were also observed for early versus late advance in sea ice but for the month of April, the month including and following the 1979/80–2013/14 mean day of advance (Figure 7 B, D, F). An early autumn advance was associated with increased ice concentrations and cold southerly winds (Figure 7B). The higher ice concentrations resulted from strong westerly winds in March (Figure 6A) driving the ice edge northward through Ekman transport. A late autumn advance was associated with decreased ice concentrations and strengthened northerly and weakened westerly winds, both contributing to stalling the ice edge advance (Figure 7 D, E). Thus, a weakening of westerly winds in March in particular (Figure 6A) is consistent with decreased autumn sea ice concentrations and later ice edge advance (Figure 3B).

The advance of the autumn ice edge is also preconditioned by the previous retreat of the spring ice edge; i.e., an earlier spring sea ice retreat creates a longer open-water interval of solar surface heating, causing a later autumn sea ice advance, while a later spring retreat leads to a shorter open-water interval of heating and an earlier autumn advance of the ice (Nihashi and Ohshima, 2001; Stammerjohn et al., 2012; Holland, 2014). In the offshore region, a later (earlier) spring sea ice retreat was often followed by an earlier (later) autumn sea ice advance (R = –0.54, Figure 3B). Thus, even when cold southerly winds would otherwise favor an early ice edge advance (e.g., the area west of 120°W in Figure 7F), sea ice growth was slowed by the additional solar heat gained by the early ice edge retreat in the preceding spring (e.g., Figure 7E).

Coastal Polynyas

Pine Island Polynya (PIP)

Over the period of 1979/80–2013/14, the duration of the ice season in the sPIP area also showed a tendency to decrease, but it was more episodic, with stepped increases in variability (Figure 8A). There was little change in ice season duration between 1979/80 and 1986/87, but that period was followed by two small excursions of shorter (by ~ 1 month) ice seasons between 1986/87 and 1994/95. Subsequently, there were two large excursions of much shorter (by ~ 3 months) ice seasons between 1995/96 and 2013/14, relative to the early 1980s. The marked increase in variability before and after 1994/95 corresponds to a significant change in the extent of the TFIT barrier that separates the PIP and ASP areas (described in detail in the Discussion section). Throughout the time series, each shortening of the ice season was largely due to an earlier spring sea ice retreat (Figure 8B), and variability in ice season duration was almost entirely explained by variability in the spring ice edge retreat (R = 0.92). There was also strong covariability between anomalies in the spring sea ice retreat and subsequent autumn advance (R = –0.76). However, anomalies in the timing of sea ice retreat were up to three times larger than those in the subsequent advance.

Much of the Amundsen Sea coast, particularly between 110°W and 120°W, experiences prevailing southeasterly winds that intensify during spring-to-autumn (Figures 4 and 6). In contrast, in the southeastern corner of the Amundsen Sea embayment region (i.e., the PIP coastal area, ~ 100°W to 110°W), the mean winds are lighter, more easterly, and more variable compared to points west of the PIP. An examination of winds and sea ice showed that when there were anomalously strong meridional winds in spring, the effect on sea ice in the PIP area was as follows. Strong southerly winds led to low sea ice concentrations and an anomalously early PIP opening, as illustrated by conditions in November 1996 (Figure 9A), November being the month when the PIP begins to open. Conversely, strong northerly winds led to high sea ice concentrations and a later PIP opening, as illustrated by conditions in November 1997 (Figure 9B). Four of the five years showing the largest anomalies in early PIP opening (1995, 1996, 2008, 2009 and 2010) experienced strong southerly winds in spring (i.e., in October and/or November). In contrast, the early opening in 1995 was not characterized by strong winds in spring, but there was a significant change to the TFIT barrier during this time (as described in the Discussion section).

We also examined variability in the location of the initial opening of the PIP, but found no distinct shift in its location over time. Given the tendency towards longer open water periods in the sPIP (Figure 8C), we then examined monthly changes in the overall size of the PIP (Figure 10) between the months of November and March. The months December to February indicated an increase in polynya size with time, albeit superimposed on large year-to-year variability. There were, however, three years when the PIP never opened in spring/summer (1985/86, 1986/87 and 2005/06). Otherwise, there was only one year (2001) when

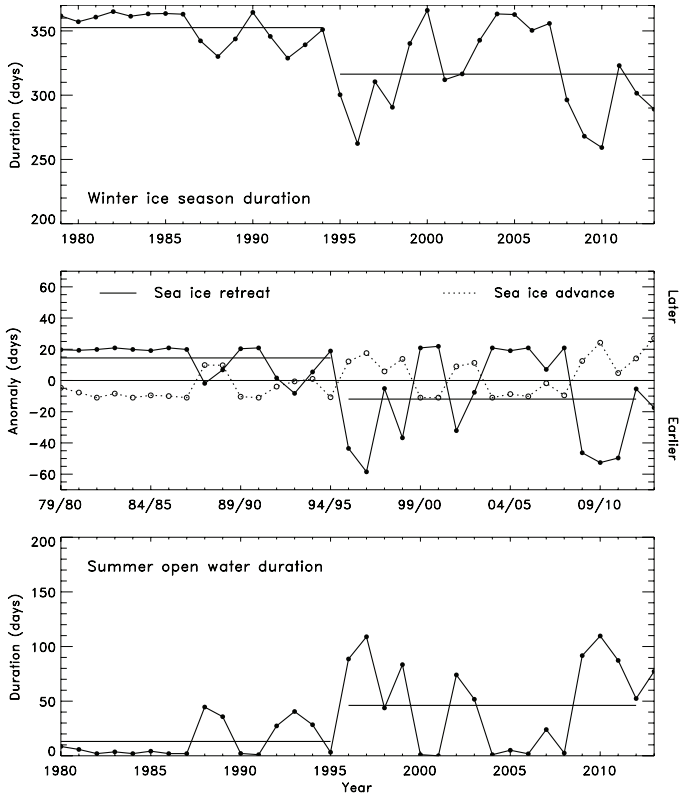

Figure 8

Ice season variability in the sPIP region.

Time series and means in the sPIP area over the period of 1979/80 to 2013/14 for: (A) sea ice season duration, (B) anomalies in the timing of sea ice retreat and subsequent advance (i.e., the times series for sea ice advance is lagged 1 year such that the austral spring–summer 1979/80 sea ice retreat is plotted against the subsequent austral autumn 1980 advance), and (C) open water duration. In (B), the temporal correlation between the de-trended time series of sea ice retreat and subsequent advance is –0.76. The two mean periods (highlighted in the duration, retreat and open water time series) correspond to the pre/post removal of the TFIT barrier separating the PIP and ASP areas. Statistics are reported in Table 1.

doi: 10.12952/journal.elementa.000055.f008

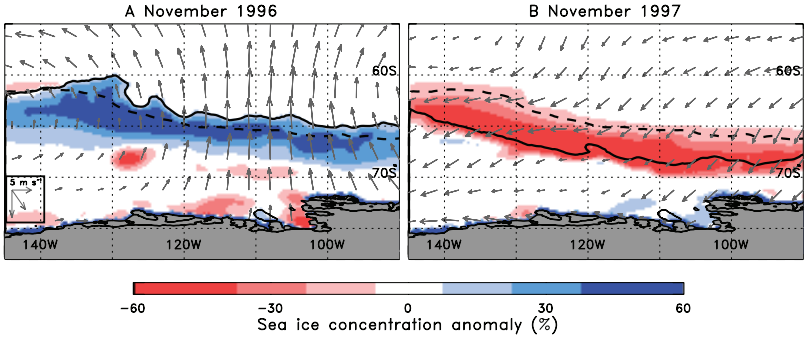

Figure 9

Anomalies in sea ice concentration and winds relevant to the coastal region.

Monthly anomalies in sea ice concentration (shading) and winds (arrows) for (A) November 1996 and (B) November 1997, showing examples of conditions leading to an early (A) versus late (B) opening in the ASP and PIP areas. The solid and dotted contours delineate the observed and 35-year mean ice edge locations, respectively (based on 15% ice concentration). A legend for the wind speed is given in the lower left corner of (A).

doi: 10.12952/journal.elementa.000055.f009

the PIP began to increase its opening as early as November (but only reached a size of 641 km^2). Typically, there was very little open water by March, but there were four years when some open water persisted (1991, 1992, 2010, 2013). During most summers, some sea ice remained offshore of the PIP (Figures 1 and 4A) except during the three highest open water summers (1991/92, 2002/03 and 2009/10), when little to no summer sea ice remained in the Amundsen Sea east of 125°W.

Amundsen Sea Polynya (ASP)

In contrast to both the offshore and sPIP areas, the seasonal sea ice decreases in the eASP region over the period of 1979/80–2013/14 resulted largely from a single shift towards shorter ice seasons (Figure 11A). The timing of this shift occurred slightly earlier (1992/93) than the 1994/95 episode noted in the sPIP time series (Figure 8). In further contrast to the sPIP, the eASP shift did not coincide with a marked increase in variability. Rather, it coincided with a decrease in fast ice extent along the western boundary of the TFIT, which exposed an area prone to early opening (as further explored below). However, similar to the sPIP, the yearly variability in ice season duration was largely explained by variability in the timing of the spring retreat (R = 0.89). But, unlike both the sPIP and offshore area, there was no significant correlation between the timing of spring retreat and subsequent autumn advance in the eASP region.

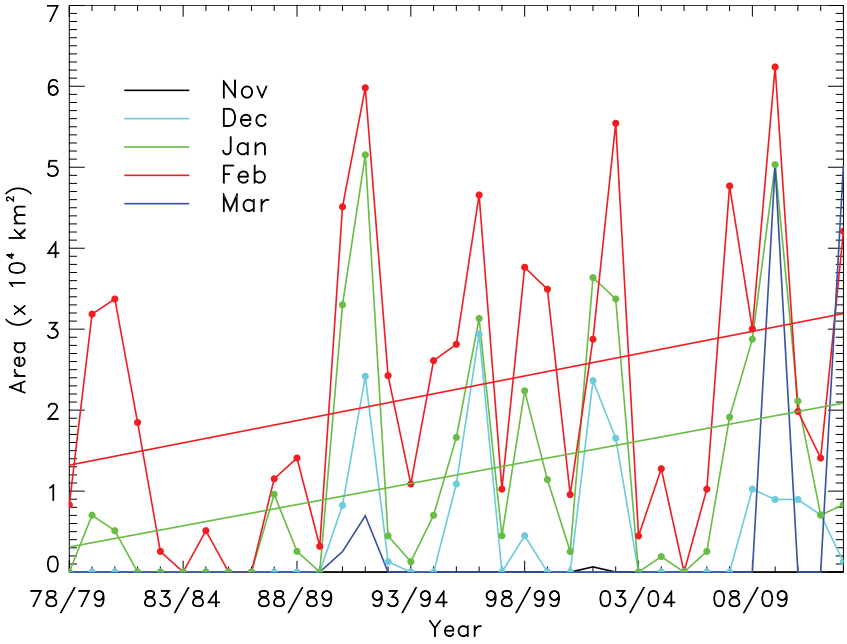

Figure 10

Variability and trends in open water area in the greater PIP region.

Time series of open water area in the greater PIP area for the months of November to March starting in 1978 for November and December, and in 1979 for January to March (and ending in 2012 and 2013, respectively). The linear trends for January (523 ± 318 km^2 yr^{-1}, $p < 0.01$) and February (551 ± 353 km^2 yr^{-1}, $p < 0.1$) are shown for reference (while trends in other months were not significant at the $p < 0.1$ level). Note that there was only one year when November showed a small open water area (the small blip in 2001 corresponding to 641 km^2).

doi: 10.12952/journal.elementa.000055.f010

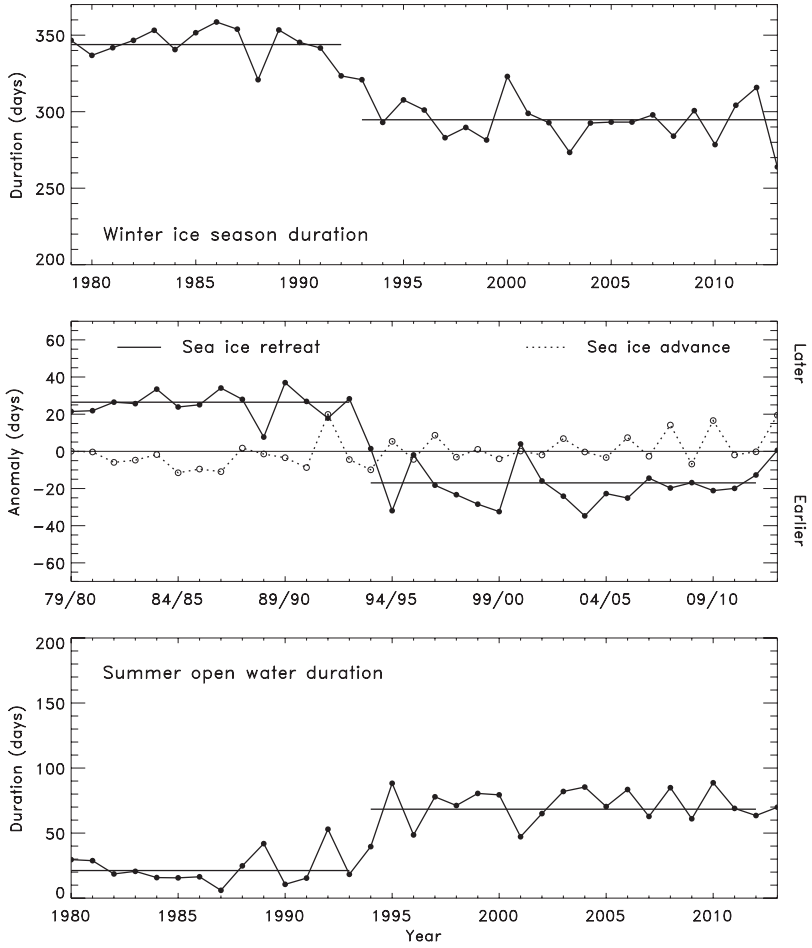

Figure 11

Ice season variability in the eASP region.

Time series and means in the eASP area over the period of 1979/80 to 2013/14 for: (A) sea ice season duration, (B) anomalies in the timing of sea ice retreat and subsequent advance (i.e., the time series for sea ice advance is lagged 1 year such that the austral spring–summer 1979/80 sea ice retreat is plotted against the subsequent austral autumn 1980 advance), and (C) summer open water duration. In (B), the temporal correlation between the de-trended time series of sea ice retreat and subsequent advance is –0.01. The two mean periods (highlighted in the duration, retreat and open water time series) correspond to the pre/post opening of the western side of the TFIT barrier. Statistics are reported in Table 1.

doi: 10.12952/journal.elementa.000055.f011

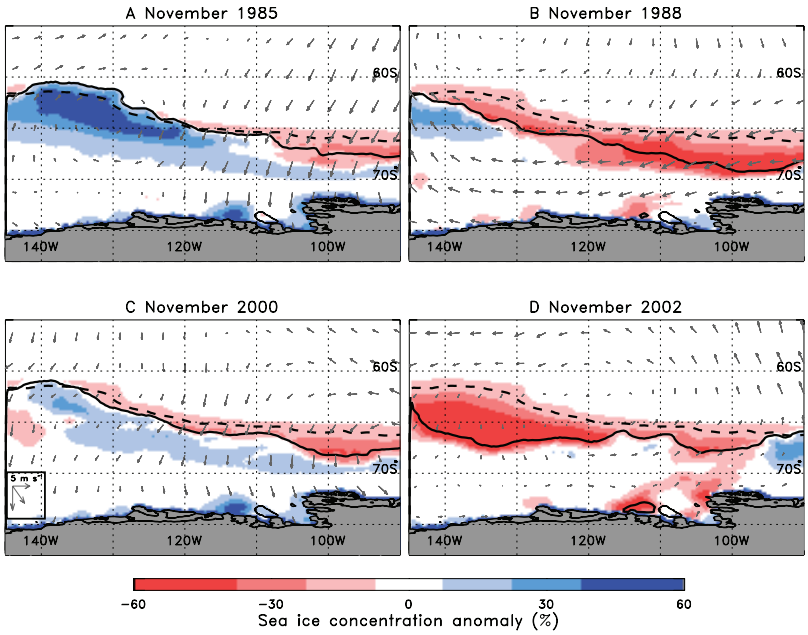

Figure 12

Anomalies in sea ice concentration and winds relevant to the eASP region.

Monthly anomalies in sea ice concentration (shading) and winds (arrows) for the November of (A) 1985, (B) 1988, (C) 2000, and (D) 2002, showing examples of conditions leading to a late (A, C) versus early (B, D) opening in the ASP area. The solid and dotted contours delineate the observed and 35-year mean ice edge locations, respectively (based on 15% ice concentration). A legend for the wind speed is given in the lower left corner of (C).

doi: 10.12952/journal.elementa.000055.f012

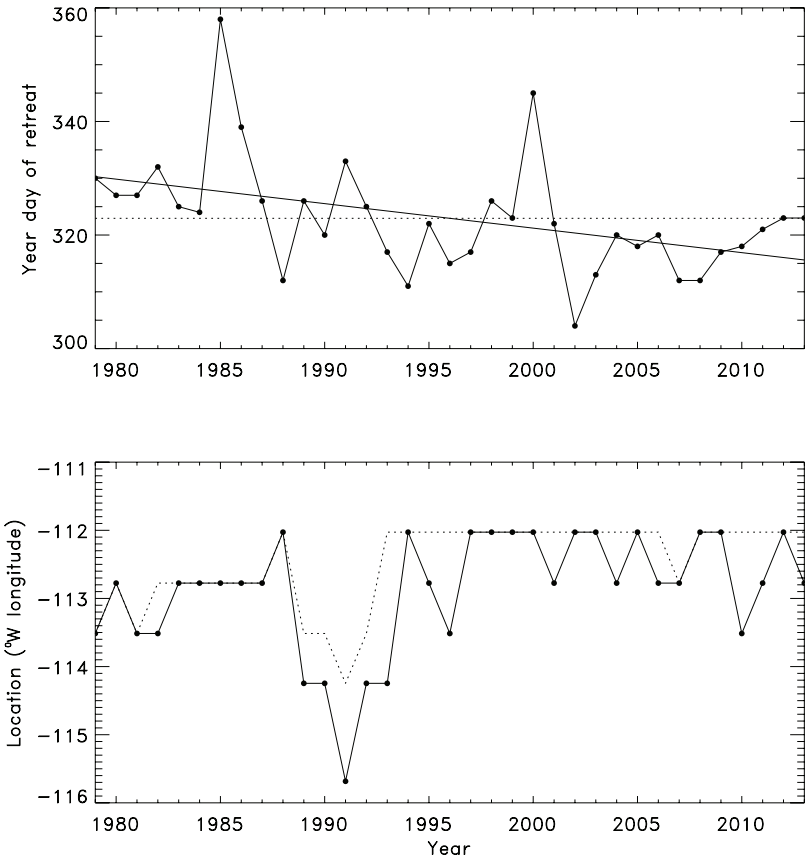

Figure 13

Variability in timing and location of the initial opening of the eASP.

Time series of (A) the earliest opening in the greater ASP area (in year day), and (B) the location (in °W longitude) of the earliest opening. If more than one pixel opened simultaneously on that day, then the furthest east (dotted) and west (solid) locations of those pixels are shown.

doi: 10.1952/journal.elementa.000055.f013

The ASP area (~ 110°W to 125°W) is exposed to some of the most persistent southeasterly winds that are observed along the Amundsen Sea coast (Figure 4) which tend to intensify during spring-to-autumn (Figure 6). However, over the period of 1979–2013 a springtime local maximum in the easterly wind was conspicuously absent during the first half of the record (Figure 6C); consequently, there was a distinct strengthening of easterly winds from August to October, with September showing the strongest trend

(–0.06 m s^{-1} yr^{-1}, $p < 0.1$). There also was a strengthening of the southerly component in June (0.06 m s^{-1} yr^{-1}, $p < 0.1$) and in October (0.04 m s^{-1} yr^{-1}, $p < 0.1$).

A strengthening of the easterly component in spring was consistent with an earlier opening of the ASP as illustrated by conditions in November 1988 (Figures 12B and 13A), which show increased open water area in the lee (i.e., west) of the TFIT barrier. When there was little to no wind anomaly (meaning there were prevailing southeasterly winds), there also was increased open water in the ASP and an early opening, as illustrated by conditions in November 2002 (Figures 12C and 13A). In contrast, when there were strong northerly wind anomalies in spring, sea ice was advected into the ASP area, increasing sea ice concentrations there and delaying its opening, as illustrated by conditions in November 1985 and 2000 (Figures 12 A, C and 13A).

During early autumn, the persistent southeasterly winds (Figure 6 C, D) were consistent with the regular closing of the greater ASP in March. During this time of year, cold winds facilitate rapid sea ice growth and closure of the ASP. Nonetheless, the persistent southeasterly winds and wind-driven advection meant that some open water was also regularly observed in the eASP, even in winter. (In comparison to the PIP, the ASP retains a larger fraction of open water during winter, with monthly-averaged sea ice concentrations reaching about 70% from April to October.)

For the greater ASP area, the initial opening of the polynya became earlier by 16 ± 7 days ($p < 0.01$) over the period of 1979/80–2013/14 (Figure 13A), but (and in contrast to the PIP) the location of that opening shifted with time (Figure 13B). Before 1989, the polynya opening was generally observed in the vicinity of 113°W, but between 1989 and 1993, it shifted further westward, to between 114 and 116°W. Post-1993, the initial opening of the polynya was generally observed in the newly opened eASP area, i.e., in the vicinity of 112°W, just west of the TFIT.

Similar to the PIP, the size of the ASP during the months of December to February also increased with time, though again superimposed on large year-to-year variability (Figure 14). In contrast to the PIP, there were no years when the ASP did not open. During the high open water years (1992, 1993, 1995, 1997, 2003, 2010), there was little to no sea ice bordering the ASP to the north and west. Otherwise, after the spring opening, some sea ice typically remained offshore of the ASP area throughout summer (Figures 1 and 4), similar to the PIP.

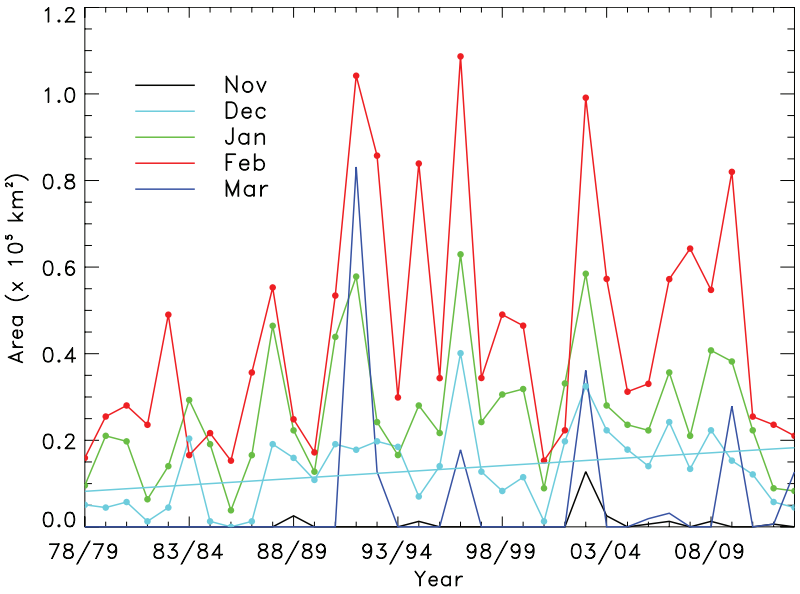

Figure 14

Variability and trends in open water area in the eASP region.

Time series of open water area in the greater ASP area for the months of November to March starting in 1978 for November and December, and in 1979 for January to March (and ending in 2012 and 2013, respectively). The linear trend for December (297 ± 186 km² yr^{-1}, $p < 0.1$) is shown for reference (while trends in other months were not significant at the $p < 0.1$ level).

doi: 10.12952/journal.elementa.000055.f014

Discussion

Prior to this study, only a few efforts have been made to examine sea ice changes specifically in the Amundsen Sea (e.g., Assmann et al., 2005). More often than not, studies combine the Amundsen and Bellingshausen seas into one sector when investigating regional and circumpolar sea ice variability (e.g., Parkinson and Cavalieri, 2012). However, there was a relatively recent study that investigated changes in phytoplankton in relation to changes in sea ice and open water variability in the two Amundsen Sea polynya areas (Arrigo et al., 2012). In that study, a higher-resolution passive microwave product (with a 6.25 km pixel size) was used to analyze data from the period of 1997–2010. Over that shorter interval, no trends or shifts were detected in the size or duration of the PIP or ASP, or in the timing of opening or closing. Instead, it was noted that interannual variability was high, especially in the smaller PIP.

Given that the seasonal sea ice changes in the offshore, sPIP and eASP areas showed only weak

co-variability with each other (as well as with the high trending areas to the east and west), these areas were likely responding differently to large-scale forcing and/or to different local forcings. Therefore, in the following sections, we discuss these local/regional differences within the context of: (i) wind-driven changes in sea ice, (ii) changes in the TFIT barrier, (iii) potential changes in upper ocean heat content, and (iv) possible causes for changes in regional atmospheric circulation.

Wind-driven changes in sea ice

Several studies have shown that sea ice variability in the West Antarctic sector is largely wind-driven (Assmann et al., 2005; Massom et al., 2008; Holland and Kwok, 2012). Given this susceptibility to wind forcing, sea ice melt and growth are preconditioned by wind-driven sea ice changes leading up to the retreat and advance, respectively. For example, the spring sea ice retreat is preconditioned by wind-driven changes in ice concentration (through wind-driven Ekman transport) occurring anytime from ~ August to ~ December. The wind-driven changes lead to higher or lower ice concentrations, and/or thicker or thinner sea ice (depending on wind direction), thus facilitating slower or faster sea ice melt and ice edge retreat (Watkins and Simmonds, 1999; Assmann et al., 2005). The subsequent autumn sea ice advance is in turn influenced by anomalies in the timing of the spring retreat via ocean thermal feedbacks, as well as by winds during the period of advance.

The Amundsen Sea is characterized by relatively fast, eastward-drifting sea ice north of ~ 71°S, with slower but persistent westward drifting sea ice to the south (e.g., Assmann et al., 2005; Holland and Kwok, 2012). Thus, the decreases in seasonal sea ice that we observed in the offshore area (between 105°W and 125°W and straddling latitudes 69 and 70°S) lie within a transition zone between fast eastward and slower westward ice motion. Earlier net sea ice transport analyses for the 1978–2001 period indicated a net annual import and melt of sea ice into the sector north of 71°S that is only partially balanced by net sea ice production and net export out of the sector south of 71°S (Assmann et al., 2005). However, our results indicate that the annual import of sea ice into the northern sector from the west (i.e., from the Ross Sea) has likely decreased since the 1978–2001 period.

With reported sea ice increases in the Ross Sea and decreases in the Bellingshausen Sea (Liu et al., 2004; Turner et al., 2009; Stammerjohn et al., 2012; Simpkins et al., 2013), the seasonal timing and strength of sea ice exchanges from the west and east have changed as well. For example, a recent analysis of "winter" (April–October) ice motion over the period of 1992–2010 shows trends of increased northward ice drift within and to the north of the northern sector (concurrent with decreased sea ice concentrations) and increased northwestward ice drift within the southern sector of the Amundsen Sea (Holland and Kwok, 2012). Both ice motion trends are coincident with the seasonal sea ice changes in the offshore and eASP areas, respectively. The increased export of sea ice out of these two areas is consistent with the observed trend towards earlier spring sea ice retreat in particular.

Given the observed decreases in winter–spring sea ice concentrations prior to retreat in these areas (Holland and Kwok, 2012; Simpkins et al., 2012), springtime meridional winds more easily drive an earlier ice edge retreat (Watkins and Simmonds, 1999). The decreased sea ice concentration is consistent with less sea ice being imported into this area from the west, coupled with the observed trend in northward ice drift out of this area (Holland and Kwok, 2012), indicating net export of sea ice out of the offshore region.

Together, these reported changes in ice motion are consistent with the observed seasonal shifts in wind speed and direction (Figure 6). For example, in the offshore area the observed delay in peak autumn westerly winds (from March to May) contributes to a later autumn sea ice advance (by northward Ekman transport), while a shorter duration peak in spring westerly winds (from July–August–September to August only) causes less sea ice to be imported from the west into the offshore region, decreased sea ice concentrations and earlier spring sea ice retreat (Figure 3). Similarly, in the eASP area, earlier and stronger peak easterly winds in spring (Figure 6C) are consistent with an earlier wind-driven opening of the polynya.

Variability in the import of sea ice from the southwestern Bellingshausen Sea also contributes to changes observed in the PIP and ASP areas. Ice motion near the coast is not well resolved by satellite (e.g., Holland and Kwok, 2012), but ice buoys deployed in the southwestern Bellingshausen Sea in March 2007 (Figure 1, inset lower right) revealed relatively fast ice speeds between the southwestern Bellingshausen Sea and the eastern Amundsen Sea. The ice drift slowed thereafter, and the drift direction became more variable as revealed by the less linear drift tracks. Sea ice originating from the southwestern Bellingshausen Sea typically consists of thick multi-year sea ice, as was the case in 2007 (Maksym, unpublished data). A thick sea ice cover on the outer continental shelf of the eastern Amundsen Sea region influences PIP and ASP variability by presenting a barrier to northward ice drift out of the PIP or ASP, thus restricting polynya size and possibly duration.

Subsequent to the arrival of ice buoys offshore of the PIP in mid-2007 (and the attendant import of thick multi-year sea ice into the eastern Amundsen Sea), the spring opening of the PIP was significantly delayed (Figure 8B), which nearly curtailed the PIP summer open water season in 2007/08 (Figure 8C). Much of the multi-year sea ice in the southern Bellingshausen Sea was removed in 2007 through the drift process described above (Stammerjohn et al., 2011), such that over the next three years there was little to no multi-year sea ice imported into the Amundsen Sea. Concurrently, over these next three years, the spring opening of the PIP was anomalously early. A similar sequence of events occurred between 1987 and 1994 in

the southern Bellingshausen Sea, when the export of thick multi-year sea ice out of the Bellingshausen Sea led to the extreme summer minima in ice extent that were observed there (Jacobs and Comiso, 1997). Again, the thick multi-year sea ice eventually moved into the eastern Amundsen Sea, but by the summer of 1995/96, much of that sea ice finally thinned out north of the PIP, leading to early openings in 1995/96 and 1996/97.

In summary, the 2-month decrease in ice season duration over the period of 1979/80–2013/14 in the offshore region coincided with seasonal shifts in wind speed and direction from March to May (relating to later advance) and from September to August (relating to earlier retreat). This coinciding pattern is consistent with observed delays in ice edge advance in autumn (i.e., delayed into April–May) and decreased net sea ice import from the west into the offshore region during early spring, leading to decreased spring sea ice concentrations and earlier ice edge retreat. In the sPIP and eASP areas, the respective episodic or step changes towards earlier spring sea ice retreat were consistent with a strengthening of southeasterly winds in September–October over the coastal region, driving earlier openings in the eASP area in particular, as well as variability in the import of thick multi-year sea ice from the southern Bellingshausen Sea into the eastern Amundsen Sea. However, as discussed next, changes to the TFIT barrier also played a significant role.

Changes in the Thwaites Fast-ice and Iceberg Tongue (TFIT)

The TFIT barrier partially bisects the Amundsen Sea coastal region, separating the PIP and ASP areas and hampering the import/export of sea ice into/out of these two areas (Figure 1). The respective episodic and step changes in the sPIP and eASP sea ice time series can thus be largely explained by variability in the TFIT barrier, acting in concert with the increases in spring southeasterly winds driving earlier spring openings in the eASP area in particular. Key changes in the TFIT barrier and their correspondence to PIP and ASP changes are highlighted below.

The Thwaites is among the fastest moving glaciers in Antarctica (Ferrigno et al., 1993; MacGregor et al., 2012; Rignot et al., 2014). It extends seaward of its grounding line, forming the Thwaites Glacier Tongue and to its north, the TFIT. At its most expansive, the northern extent of the TFIT complex extends up to 250 km seaward of the Thwaites grounding line (Swithinbank, 1988). The TFIT barrier has been a highly variable feature over at least the last 70 years (Ferrigno et al., 1993; MacGregor et al., 2012). In the 1970s and 1980s, the Thwaites Iceberg Tongue was composed of tabular iceberg B10 (~ 80 km by ~ 40 km; not christened B10 until 1992), grounded just to the north of the Thwaites Glacier Tongue and connected via fast ice and smaller icebergs (Ferrigno et al., 1993). In 1986, however, B10 shifted slightly northward, leaving an approximate 30 km distance of open water between the iceberg and glacier tongue. Between 1986 and 1990, B10 shifted northward again and rotated east–west, drifting approximately 80 km westward to a position north of the Martin and Bear peninsulas, i.e., in the northern ASP area. Over the next two years, it drifted another 60 km west, and then left the Amundsen Sea in the mid-1990s.

As of February 2015, the northern portion of the Thwaites Iceberg Tongue was composed of a large tabular iceberg B22A (82 km long by 44 km wide) that calved from the Thwaites Glacier Tongue in 2002 (http://www.publicaffairs.noaa.gov/releases2002/mar02/noaa02026.html). Since December 2010, a newer southern portion of the Thwaites Iceberg Tongue has been composed of B29 (9 km by 20 km) and B28 (13 km by 19 km) (http://www.natice.noaa.gov/pub/icebergs/Iceberg_Tabular.pdf), resulting from a calving event within 16 km of the Thwaites grounding line (MacGregor et al., 2012). Since the 2010 calving event, the TFIT complex has been quite variable, particularly at its southern extent due to rapid changes in the glacier tongue. (A link to an animation showing the changes described above can be found in MacGregor et al., 2012: see Table 1, Animation 1.) Recent reports indicate that this area will continue to be quite variable, given the rapid retreat of the Thwaites grounding line, with future retreat likely due to the absence of pinning points upstream of the current grounding line (Rignot et al., 2014).

The spatial extent of the TFIT barrier has an obvious influence on the circulation of sea ice in both the PIP and ASP areas. The westward movement of B10 between 1986 and 1990 was concurrent with seasonal sea ice decreases observed in the sPIP (Figure 8A). The continued westward movement and eventual departure of B10 from the PIP/ASP area between 1990 and 1995 was also coincident with marked episodic decreases in seasonal sea ice in the sPIP (Figure 8), as well as the step change in the eASP time series that resulted in a 2-month decrease in ice season duration (Figure 11A). Additionally, the increase in easterly winds over the coastal area in the mid-1990s (Figure 6C) coincided with earlier openings of the eASP (Figure 11), whereas the wind-driven westward ice motion out of the PIP was periodically blocked whenever the TFIT barrier was more extensive (e.g., the expansion of the glacier tongue between the mid-1990s to mid-2000s that then calved to produce B22 in 2002).

Potential changes in upper ocean heat content

Although winds and coastal icescape changes play a large role in explaining sea ice variability in the three areas, other factors come into play as well. The generally high correspondence between anomalies in the spring sea ice retreat and the subsequent autumn advance, as revealed in the offshore and sPIP time series

(Table 1), suggests that changes in the autumn advance may also be due to an ocean thermal feedback (Nihashi and Ohshima, 2001; Stammerjohn et al., 2012; Holland, 2014). With an earlier spring sea ice retreat, there is a net gain in solar warming of the upper ocean by end of summer that in turn delays the onset of freezing in autumn. Even with favorable (i.e., cold southerly) winds in autumn, ice formation is delayed by the additional time needed to cool the relatively warmer mixed layer (e.g., Figure 7F) (Stammerjohn et al., 2011). That there was little relationship between the spring retreat and subsequent advance in the eASP region was due to the persistent southeasterly winds blowing over the TFIT that helped maintain the dominance of wind-driven dynamics, particularly in spring.

In the coastal area, additional factors contribute to sea ice changes, particularly in sea ice thickness. The PIP and ASP are generally categorized as wind-driven latent heat polynyas. Airflow over the ASP in particular (Figure 4) is characterized by strengthened katabatic winds converging along confluences in ice sheet topography (Parish and Bromwich, 2007). However, the upwelling or mixing of warm CDW into surface waters in the PIP and ASP areas provides a sensible heat component as well (Mankoff et al., 2012).

Cooled and freshened CDW, exiting from under the Pine Island and Dotson ice shelves (and from other ice shelves in the Amundsen Sea embayment region), has been made buoyant by basal ice shelf melt and also retains some residual heat, with temperatures a few degrees above freezing (Jacobs et al., 2012). Whether warm, freshened CDW mixes with surface waters in the PIP and ASP areas to provide enough of a sensible heat or freshwater component to affect the overlying ice cover depends on several factors, including winds, tidal forcing, ocean stratification, sub-ice shelf circulation, and eddy activity on the continental shelf. The latter three factors are quite variable in the Amundsen Sea region (Jacobs et al., 2012; St-Laurent et al., 2013; Dutrieux et al., 2014), while tidal forcing contributes to mixing in front of and under the Pine Island and Dotson ice shelves, thus contributing to changes in basal ice shelf melt (Robertson, 2013).

With regards to wind-induced mixing, an analysis of Ekman pumping indicates that the greater PIP and ASP areas regularly experience upwelling (Ekman suction) particularly from August to October (Yuan, personal communication). However, the central Amundsen Sea, including the coastal ASP area, is weakly stratified (compared to the PIP area in the eastern Amundsen Sea), indicating that wind-induced mixing of meltwater-modified CDW is a possibility. An analysis of freshwater distributions in the ASP area shows relatively high fractions of meteoric water (2–3%) throughout the deep winter mixed layers, the main source of which appears to be from basal ice shelf melt (Randall-Goodwin et al., 2015).

If upwelling of warm CDW caused an increase in upper ocean heat content, then this factor would affect sea ice by potentially delaying the onset of sea ice growth in autumn and limiting its thickness in winter, which in turn would promote earlier melt-back in spring. The seasonal sea ice trends in the sPIP and eASP areas are consistent with that scenario, but to test it would require year-round coincident in situ observations of sea ice mass balance and water column changes, a difficult proposition in these highly dynamic, coastal polynya environments.

To date, there has been just one 6-week joint deployment of an ice mass balance buoy (IMB; Perovich et al., 2004) and an ice-tethered profiler (ITP; Toole et al., 2011) in the Amundsen Sea (Ackley et al., 2015). In that study, the ITP and IMB were installed within 50 m of each other on fast ice near the TFIT during February–March of 2009. The ITP collected water column temperature and salinity profiles between 7-m and 760-m depths each day, while the IMB collected snow/ice thickness changes, temperature profiles through the snow and sea ice, and temperature and salinity at ~ 1.2 m below the sea ice; both packages relayed their data by Iridium Satellite. Average ocean heat flux of ~ 17 W m^{-2} was estimated by the total ice thickness change recorded by the IMB, with periods of more intense ocean heat flux (up to 56 W m^{-2}) and higher ice melt corresponding with several CDW upwelling events as captured by the ITP profiles. Although limited in space and time, this study provides evidence that sea ice thickness in the Amundsen Sea coastal area can be affected by CDW upwelling.

Possible causes for the regional atmospheric circulation changes

Mean seasonal changes in winds (Figure 4), as well as changes documented over the period of 1979–2013 (Figures 6), are differently timed between the offshore and coastal areas, suggesting different local forcing and/or response to large-scale forcing. Coastal winds are influenced by katabatic drainage off the continent (in response to diabatic cooling of sloped ice surfaces) and by synoptic variability (Parish and Bromwich, 2007), while offshore winds, particularly in the Amundsen Sea sector, are influenced by high synoptic variability. However, both are influenced by large-scale climate variability. Of related interest is that, on a year-to-year basis when offshore northwesterly wind speed is relatively high, the coastal southeasterly wind speed is relatively low, and vice-versa (Figure 5).

Changes in seasonal peak winds in the offshore region from March to May and from September to August (Figure 6A), and the consequent impact on delaying the autumn ice edge advance and accelerating its spring retreat, respectively, suggest a modification of the Semi-Annual Oscillation (SAO) (Turner et al., 2013). The SAO is a twice-yearly poleward contraction (spring, autumn) and equatorward expansion (summer, winter) of the circumpolar low-pressure belt (van Loon, 1967). Changes in SAO-like behavior in

the Amundsen Sea could be influenced by a number of factors, including those factors affecting the seasonal location of the Amundsen Sea Low (ASL). The ASL is a prominent feature of the regional atmospheric circulation in the West Antarctic sector, where it forms a semi-permanent low-pressure system located within the Bellingshausen-Amundsen-Ross Seas sector (Fogt et al., 2012; Hosking et al., 2013; Turner et al., 2013). The climatological location and strength of the ASL changes seasonally. In January, it is furthest north and east (~ 67°S and ~ 110°W); in June, it is furthest south and west (~ 72°S and ~ 150°W). During autumn and spring, the ASL is located in the western Amundsen Sea in the vicinity of 130°W, where it is a bit further north (~ 69–70°S) in autumn (March–April) and more south (~ 70–71°S) in late winter–spring (August–November) (Turner et al., 2013).

Various climate modes affect the location and intensity of the ASL, including the Southern Annual Mode (SAM), the high-latitude atmospheric response to El Niño-Southern Oscillation (ENSO) and zonal wave variability (e.g., Yuan and Li, 2008; Hobbs and Raphael, 2010; Raphael and Hobbs, 2014). Recent findings also indicate that the leading mode of tropical and North Atlantic sea surface temperature (SST) variability, the Atlantic Multi-decadal Oscillation (AMO), affects atmospheric circulation in the West Antarctic sector (Li et al., 2014) through similar teleconnections to ENSO (i.e., Rossby wave propagation of atmospheric perturbations).

Changes in the seasonal position and intensity of the ASL strongly influence wind-driven sea ice changes in the Amundsen Sea. If the ASL is positioned north or south of the ice edge, then easterly or westerly winds prevailing along the southern or northern limb of the ASL will affect the ice edge location and sea ice concentrations inside the ice edge. Similarly, if the ASL is positioned east or west of an area in question, then southerly or northerly winds prevailing along the western or eastern limb of the ASL will affect sea ice concentrations in the area in question. Finally, if the ASL is intensified (i.e., deepened), then these winds become anomalously stronger. A positive (negative) SAM in summer–autumn intensifies (weakens) the ASL poleward, while the high-latitude response to La Niña (El Niño) intensifies (weakens) the ASL and moves it slightly westward (eastward) in winter–spring (Turner et al., 2013). Of relevance to the Amundsen Sea in particular, the ASL also has intensified over the last ~ 30 years during autumn and spring (i.e., when the ASL is typically in the western Amundsen Sea) in accord with an increase in the amplitude of the SAO (Turner et al., 2013).

The SAO-related changes are consistent with the observed changes in winds. The increase (decrease) in westerly (northerly) winds in the offshore area in May (Figure 6 A, B) correspond to a southeastward shift in an intensified ASL. In contrast, the decrease (increase) in westerly (northerly) winds in September corresponds to a northwestward shift in an intensified ASL. The latter also coincided with an increase in easterly winds over the coastal area (Figure 6C). However, the overall increase in easterly winds in the coastal area during winter and spring could also be due to an increase in the number of La Niña events during the period of 1996–2012 as compared to 1979–1995 (9 versus 3 yearly events, respectively, based on our interpretation of the Oceanic Niño Index). As mentioned, the ASL strengthens during La Niña (Turner et al., 2013), which in turn would lead to an increase in easterly winds over the coastal area.

A final point is that sea ice changes in the Amundsen Sea region were comparatively weaker and less spatially coherent than in the Bellingshausen and western Ross Sea regions over the period examined. These latter two high-trending sea ice areas are east and west, respectively, of the area showing the largest atmospheric synoptic variability (e.g., Simmonds et al., 2003; Fogt et al., 2012). Not only is synoptic variability particularly high in the Amundsen Sea, but also, as described above, air-sea-ice interactions are quite sensitive to the seasonally expressed, but differently timed, climate modes and tropical teleconnections. Therefore, it is not surprising that sea ice changes in the Amundsen Sea, as described in this study, were spatially variable and differently timed, compared to the sea ice changes to the east and west of the Amundsen Sea area.

Conclusions

Over the period of 1979–2014 three areas in the Amundsen Sea showed notable seasonal sea ice decreases that occurred either gradually (in the offshore region; Figure 3), episodically (in the sPIP region; Figure 8), or as a single shift (in the eASP region; Figure 11). The seasonal sea ice decreases in the offshore area occurred more or less monotonically with time, resulting in a 2-month shorter ice season over the last 35 years (Figure 3). In contrast, in the sPIP area the ice season decreased by 1 to 3 months during roughly five different episodes over the 35-year period (Figure 8). In the eASP area, the ice season decreased by 2 months in a single step that occurred in the mid-1990s (Figure 11).

In the offshore region, ice season decreases were due to changes in both spring sea ice retreat and autumn advance. An earlier spring sea ice retreat was associated with decreased (increased) westerly (northerly) winds in September (and decreased ice import from the west) (Assmann et al., 2005; Holland and Kwok, 2012) followed by strengthening of northerly winds in spring. A later autumn sea ice advance was associated with weakening of westerly winds in March, as well as ocean thermal feedbacks in response to earlier spring retreat. The wind changes corresponded to shifts in peak winds from March and September to May

and August that were consistent with reported changes in the location and intensity of the Amundsen Sea Low (Turner et al., 2013).

In contrast, the sea ice decreases in the sPIP and eASP areas were due mostly to changes in spring sea ice retreat, associated with episodic changes in the extent of the TFIT barrier (separating the PIP and ASP areas), as well as increased southeasterly winds over the coastal region. Variability in the import of thick multi-year sea ice from the southern Bellingshausen Sea into the eastern Amundsen Sea, together with variability in the number of icebergs on the outer continental shelf that retain summer sea ice, were other factors contributing to PIP/ASP variability. The sPIP and eASP sea ice changes are important, as they affect the timing, duration and size of these two polynyas and thus impact this biologically productive area (Arrigo and van Dijken, 2003; Arrigo et al., 2012; Alderkamp et al., 2015; Mu et al., 2015), as well as possibly indicating a response to changes in heat and freshwater inputs (Randall-Goodwin et al., 2015; Sherrell et al., 2015).

Temporal correlations were weak between sea ice variability in the three Amundsen Sea areas, as well as between the Amundsen Sea and the two high-trending areas to the east and west (in the Bellingshausen and western Ross seas, respectively). The lack of covariability suggests that the sea ice changes in the Amundsen Sea are responding differently to large-scale forcing and/or to different local forcing. Air-ocean-ice interactions in the Amundsen Sea are influenced by various climate modes and are highly sensitive to tropical forcing. Such influences act on the ASL, a semi-permanent low-pressure system located within the Bellingshausen-Amundsen-Ross Seas sector (Fogt et al., 2012; Hosking et al., 2013; Turner et al., 2013). The ASL has intensified over the last ~ 30 years during autumn and spring, the same seasons when it is typically located in the western Amundsen Sea (Turner et al., 2013). These changes in the seasonal intensity and location of the ASL are consistent with the observed sea ice and wind changes reported here.

Although the sea ice changes observed in the offshore and coastal polynya areas were consistent with changes in winds and to the coastal icescape, for the coastal polynya areas an additional but unknown factor is how sea ice is responding to changes in ocean heat and freshwater inputs. Such changes may be resulting from longer summer open-water periods, variability in ice-shelf melt, and variability in the relatively warm buoyant waters exiting the ice-shelf cavities (for example). Currently, we lack sufficient in situ time series data to investigate changes in ice-ocean interactions over time, but a short deployment of a co-located ice mass balance buoy and ice-tethered profiler in January-March of 2009 shows episodes of sea ice basal melt and thinning in response to CDW upwelling events (Ackley et al., 2015).

Unraveling cause and effect of sea ice changes in the Amundsen Sea presents some key challenges, made more relevant given recent reports of climate-sensitive ice-shelf melting (Dutrieux et al., 2014; Paolo et al., 2015) and the rapid retreat of grounding lines in the Amundsen Sea embayment area (Mouginot et al., 2014; Rignot et al., 2014). This work underscores the need for improved and coordinated in situ time series observations of air-ocean-ice interactions, coupled with continued improvements in satellite-derived products and high-resolution ocean models. Although acquiring in situ observations is challenging, given the highly dynamic nature of Antarctic sea ice, newer, cost-effective and more sophisticated technologies (e.g., autonomous vehicles and moored instrumentation) are now making such observations possible (Schofield et al., 2010, 2015; Maksym et al., 2012; Smith et al., 2014; Ackley et al., 2015; Ducklow et al., 2015). By joining these efforts, we will better resolve cause and effect and better assess future changes to this highly sensitive and rapidly changing marine environment.

References

Ackley SF, Xie H, Tichenor EA. 2015. Ocean heat flux under Antarctic sea ice in the Bellingshausen and Amundsen Seas: two case studies. *Ann Glaciol* **56**: 200–210. doi:10.3189/2015AoG69A890.

Alderkamp A-C, Dijken GL, Lowry KE, Connelly TL, Lagerstrom M, et al. 2015. Fe availability drives phytoplankton photosynthesis rates during spring bloom in the Amundsen Sea Polynya, Antarctica. *Elem Sci Anth* **2**: 000043 doi: 10.12952/journal.elementa.000043.

Arneborg L, Wåhlin AK, Björk G, Liljebladh B, Orsi AH. 2012. Persistent inflow of warm water onto the central Amundsen shelf. *Nat Geosci* **5**: 876–880. doi:10.1038/ngeo1644.

Arrigo KR, Lowry KE, van Dijken GL. 2012. Annual changes in sea ice and phytoplankton in polynyas of the Amundsen Sea, Antarctica. *Deep Sea Res Pt II* **71–76**: 5–15. doi:10.1016/j.dsr2.2012.03.006.

Arrigo KR, van Dijken GL. 2003. Phytoplankton dynamics within 37 Antarctic coastal polynya systems. *J Geophys Res* **108**: doi:10.1029/2002jc001739.

Assmann KM, Hellmer HH, Jacobs SS. 2005. Amundsen Sea ice production and transport. *J Geophys Res* **110**: doi:10.1029/2004jc002797.

Assmann KM, Jenkins A, Shoosmith DR, Walker DP, Jacobs SS, et al. 2013. Variability of Circumpolar Deep Water transport onto the Amundsen Sea Continental shelf through a shelf break trough. *J Geophys Res-Oceans* **118**: 6603–6620. doi:10.1002/2013jc008871.

Bracegirdle TJ. 2013. Climatology and recent increase of westerly winds over the Amundsen Sea derived from six reanalyses. *Int J Climatol* **33**: 843–851. doi:10.1002/joc.3473.

Comiso JC. 2000. Variability and trends in Antarctic surface temperatures from in situ and satellite infrared measurements. *J Climate* **13**: 1674–1696.

Comiso JC. 2010. *Polar Oceans from Space*. Springer.
Comiso JC, Cavalieri D, Parkinson C, Gloersen P. 1997. Passive microwave algorithms for sea ice concentration - a comparison of two techniques. *Remote Sens Environ* **60**: 357–384.
Comiso JC, Nishio F. 2008. Trends in the sea ice cover using enhanced and compatible AMSR-E, SSM/I, and SMMR data. *J Geophys Res* **113**: doi:10.1029/2007JC004257.
Dee DP, Uppala SM, Simmons AJ, Berrisford P, Poli P, et al. 2011. The ERA-Interim reanalysis: configuration and performance of the data assimilation system. *Q J Roy Meteor Soc* **137**: 553–597. doi:10.1002/qj.828.
Dinniman MS, Klinck JM, Hofmann EE. 2012. Sensitivity of Circumpolar Deep Water transport and ice shelf basal melt along the West Antarctic Peninsula to changes in the winds. *J Climate* **25**: 4799–4816. doi:10.1175/jcli-d-11-00307.1.
Ducklow HW, Wilson SE, Post AF, Stammerjohn SE, Erickson M, et al. 2015. Particle flux on the continental shelf in the Amundsen Sea Polynya and Western Antarctic Peninsula. *Elem Sci Anth* **2**: 000046 doi: 10.12952/journal.elementa.000046.
Dutrieux P, De Rydt J, Jenkins A, Holland PR, Ha HK, et al. 2014. Strong sensitivity of Pine Island ice-shelf melting to climatic variability. *Science* **343**: 174–178. doi:10.1126/science.1244341.
Eisenman I, Meier WN, Norris JR. 2014. A spurious jump in the satellite record: is Antarctic sea ice really expanding? *The Cryosphere Discuss* **8**: 273–288. doi:10.5194/tcd-8-273-2014.
Ferrigno JG, Lucchitta BK, Mullins KF, Allison AL, Allen RJ, et al. 1993. Velocity measurentents and changes in position of Thwaites Glacier/iceberg tongue from aerial photo graphy, Landsat images and NOAA AVHRR data. *Ann Glaciol* **17**: 239–244.
Fogt RL, Wovrosh AJ, Langen RA, Simmonds I. 2012. The characteristic variability and connection to the underlying synoptic activity of the Amundsen-Bellingshausen Seas Low. *J Geophys Res-Atmos* **117**: n/a-n/a. doi:10.1029/2011jd017337.
Fraser AD, Massom RA, Michael KJ, BK G-F, Lieser JL. 2012. East Antarctic landfast sea ice distribution and variability, 2000-08. *J Climate* **25**: 1137–1156.
Haran T, Bohlander J, Scambos T, Painter T, Fahnestock M. 2014. MODIS Mosaic of Antarctica 2008–2009 (MOA2009) Image Map [Coastlines, Grounding Lines, and Islands]. (http://dx.doi.org/10.7265/N5KP8037)
Hobbs WR, Raphael MN. 2010. The Pacific zonal asymmetry and its influence on Southern Hemisphere sea ice variability. *Antarct Sci* **22**: 559–571. doi:10.1017/s0954102010000283.
Holland PR. 2014. The seasonality of Antarctic sea ice trends. *Geophys Res Lett* **41**: 4230–4237. doi:10.1002/2014gl060172.
Holland PR, Kwok R. 2012. Wind-driven trends in Antarctic sea-ice drift. *Nat Geosci* **5**: 872–875. doi:10.1038/ngeo1627.
Hosking JS, Orr A, Marshall GJ, Turner J, Phillips T. 2013. The influence of the Amundsen–Bellingshausen Seas Low on the climate of West Antarctica and its representation in coupled climate model simulations. *J Climate* **26**: 6633–6648. doi:10.1175/jcli-d-12-00813.1.
Jacobs SS, Comiso JC. 1993. A recent sea-ice-retreat west of the Antarctic Peninsula. *Geophys Res Lett* **20**: 1171–1174.
Jacobs SS, Comiso JC. 1997. Climate variability in the Amundsen and Bellingshausen Seas. *J Climate* **10**: 697–709.
Jacobs SS, Jenkins A, Giulivi CF, Dutrieux P. 2011. Stronger ocean circulation and increased melting under Pine Island Glacier ice shelf. *Nat Geosci* **4**: 519–523. doi:10.1038/ngeo1188.
Jacobs SS, Jenkins A, Hellmer H, Giulivi C, Nitsche F, et al. 2012. The Amundsen Sea and the Antarctic Ice Sheet. *Oceanogr* **25**: 154–163. doi:10.5670/oceanog.2012.90.
Jenkins A, Dutrieux P, Jacobs SS, McPhail SD, Perrett JR, et al. 2010. Observations beneath Pine Island Glacier in West Antarctica and implications for its retreat. *Nat Geosci*: doi: 10.1038/ngeo1890.
Kwok R, Maksym T. 2014. Snow depth of the Weddell and Bellingshausen sea ice covers from IceBridge surveys in 2010 and 2011: An examination. *J Geophys Res-Oceans* **119**: 4141–4167. doi:10.1002/2014jc009943.
Li X, Holland DM, Gerber EP, Yoo C. 2014. Impacts of the north and tropical Atlantic Ocean on the Antarctic Peninsula and sea ice. *Nature* **505**: 538–542. doi:10.1038/nature12945.
Liu J, Curry JA, Martinson DG. 2004. Interpretation of recent Antarctic sea ice variability. *Geophys Res Lett* **31**: doi:10.1029/2003GL018732.
MacGregor JA, Catania GA, Markowski MS, Andrews AG. 2012. Widespread rifting and retreat of ice-shelf margins in the eastern Amundsen Sea Embayment between 1972 and 2011. *J Glaciol* **58**: 458–466. doi:10.3189/2012JoG11J262.
Maksym T, Stammerjohn S, Ackley S, Massom R. 2012. Antarctic sea ice—A polar opposite? *Oceanogr* **25**: 140–151. doi:10.5670/oceanog.2012.88.
Mankoff KD, Jacobs SS, Tulaczyk SM, Stammerjohn SE. 2012. The role of Pine Island Glacier ice shelf basal channels in deep-water upwelling, polynyas and ocean circulation in Pine Island Bay, Antarctica. *Ann Glaciol* **53**: 123–128. doi:10.3189/2012AoG60A062.
Maslanik J, Stroeve J. 1999. Near-Real-Time DMSP SSM/I Daily Polar Gridded Sea Ice Concentrations 2008. Boulder, Colorado USA: National Snow and Ice Data Center. Digital Media.
Massom RA, Hill KL, Lytle VI, Worby AP, Paget MJ, et al. 2001. Effects of regional fast-ice and iceberg distributions on the behavior of the Mertz Glacier polynya, East Antarctica. *Ann Glaciol* **33**: 391–398.
Massom RA, Stammerjohn SE, Lefebvre W, Harangozo SA, Adams N, et al. 2008. West Antarctic Peninsula sea ice in 2005: Extreme compaction and ice edge retreat due to strong anomaly with respect to climate. *J Geophys Res* **113**: doi:10.1029/2007JC004239.
Mouginot J, Rignot E, Scheuchl B. 2014. Sustained increase in ice discharge from the Amundsen Sea Embayment, West Antarctica, from 1973 to 2013. *Geophys Res Lett* **41**: 1576–1584. doi:10.1002/2013gl059069.
Mu L, Stammerjohn SE, Lowry KE, Yager PL. 2015. Spatial variability of surface pCO_2 and air-sea CO_2 flux in the Amundsen Sea Polynya, Antarctica. *Elem Sci Anth* **2**: 1–19. doi:10.12952/journal.elementa.000036.
Nihashi S, Ohshima KI. 2001. Relationship between the sea ice cover in the retreat and advance seasons in the Antarctic Ocean. *Geophys Res Lett* **28**: 3677–3680. doi:10.1029/2001gl012842.
Nihashi S, Ohshima KI. 2015. Circumpolar mapping of Antarctic coastal polynyas and landfast sea ice: relationship and variability. *J Clim*: in press.

Nitsche FO, Jacobs SS, Larter RD, Gohl K. 2007. Bathymetry of the Amundsen Sea continental shelf: Implications for geology, oceanography, and glaciology. *Geochem Geophys Geosyst* **8**: 1–10. doi:10.1029/2007gc001694.

Paolo FS, Fricker HA, Padman L. 2015. Volume loss from Antarctic ice shelves is accelerating. *Science*: doi:10.1126/science.aaa0940.

Parish TR, Bromwich DH. 2007. Reexamination of the near-surface airflow over the Antarctic continent and implications on atmospheric circulations at high southern latitudes. *Mon Weather Rev* **135**: 1961–1973. doi:10.1175/mwr3374.1.

Parkinson CL. 2004. Southern Ocean sea ice and its wider linkages: insights revealed from models and observations. *Antarct Sci* **16**: 387–400.

Parkinson CL, Cavalieri DJ. 2012. Antarctic sea ice variability and trends, 1979–2010. *The Cryosphere Discuss* **6**: 931–956. doi:10.5194/tcd-6-931-2012.

Perovich DK, Elder BC, Claffey KJ, Stammerjohn S, Smith R, et al. 2004. Winter sea ice properties in Marguerite Bay, Antarctica. *Deep-Sea Res Pt II* **51**: 2023–2039.

Petty AA, Holland PR, Feltham DL. 2014. Sea ice and the ocean mixed layer over the Antarctic shelf seas. *The Cryosphere Discuss* **8**: 761–783. doi:10.5194/tc-8-761-2014.

Pritchard HD, Ligtenberg SR, Fricker HA, Vaughan DG, van den Broeke MR, et al. 2012. Antarctic ice-sheet loss driven by basal melting of ice shelves. *Nature* **484**: 502–505. doi:10.1038/nature10968.

Randall-Goodwin E, Meredith MP, Jenkins A, Sherrell RM, et al. 2015. Water mass structure and freshwater distributions in the Amundsen Sea Polynya, Antarctica. *Elem Sci Anth*: Under review for this Special Feature.

Raphael MN, Hobbs W. 2014. The influence of the large-scale atmospheric circulation on Antarctic sea ice during ice advance and retreat seasons. *Geophys Res Lett* **41**: 5037–5045. doi:10.1002/2014gl060365.

Rignot E, Jacobs S, Mouginot J, Scheuchl B. 2013. Ice-shelf melting around Antarctica. *Science* **341**: 266–270. doi:10.1126/science.1235798.

Rignot E, Mouginot J, Morlighem M, Seroussi H, Scheuchl B. 2014. Widespread, rapid grounding line retreat of Pine Island, Thwaites, Smith, and Kohler glaciers, West Antarctica, from 1992 to 2011. *Geophys Res Lett* **41**: 3502–3509. doi:10.1002/2014gl060140.

Robertson R. 2013. Tidally induced increases in melting of Amundsen Sea ice shelves. *J Geophys Res-Oceans* **118**: 3138–3145. doi:10.1002/jgrc.20236.

Santer BD, Wigley TML, Boyle JS, Gaffen DJ, Hnilo JJ, et al. 2000. Statistical significance of trends and trend differences in layer-average atmospheric temperature time series. *J Geophys Res* **105**: 7337–7356.

Schofield O, Ducklow HW, Martinson DG, Meredith MP, Moline MA, et al. 2010. How do polar marine ecosystems respond to rapid climate change? *Science* **328**: doi: 10.1126/science.1185779.

Schofield O, Miles T, Alderkamp A-C, Lee SH, Haskins C, et al. 2015. In situ phytoplankton distributions in the Amundsen Sea polynya measured by autonomous gliders. *Elem Sci Anth*: Under review for this Special Feature.

Sherrell RM, Lagerstrom M, Forsch KO, Stammerjohn SE, Yager PL. 2015. Dynamics of dissolved iron and other bioactive trace metals (Mn, Ni, Cu, Zn) in the Amundsen Sea Polynya, Antarctica. *Elem Sci Anth*: Under review for this Special Feature.

Simmonds I, Keay K, Lim E-P. 2003. Synoptic activity in the seas around Antarctica. *Mon Weather Rev* **131**: 272–288.

Simpkins GR, Ciasto LM, England MH. 2013. Observed variations in multidecadal Antarctic sea ice trends during 1979–2012. *Geophys Res Lett* **40**: 3643–3648. doi:10.1002/grl.50715.

Simpkins GR, Ciasto LM, Thompson DWJ, England MH. 2012. Seasonal relationships between large-scale climate variability and Antarctic sea ice concentration. *J Climate* **25**: 5451–5469. doi:10.1175/jcli-d-11-00367.1.

Simpkins GR, McGregor S, Taschetto AS, Ciasto LM, England MH. 2014. Tropical connections to climatic change in the extratropical Southern Hemisphere: The role of Atlantic SST trends. *J Climate* **27**: 4923–4936. doi:10.1175/jcli-d-13-00615.1.

Smith W, Goetz K, Kaufman D, Queste B, Asper V, et al. 2014. Multiplatform, multidisciplinary investigations of the impacts of modified Circumpolar Deep Water in the Ross Sea, Antarctica. *Oceanogr* **2**: doi:10.5670/oceanog.2014.36.

St-Laurent P, Klinck JM, Dinniman MS. 2013. On the role of coastal troughs in the circulation of warm Circumpolar Deep Water on Antarctic shelves. *J Phys Oceanogr* **43**: 51–64. doi:10.1175/jpo-d-11-0237.1.

Stammerjohn S, Massom R, Rind D, Martinson D. 2012. Regions of rapid sea ice change: An inter-hemispheric seasonal comparison. *Geophys Res Lett* **39**: n/a-n/a. doi:10.1029/2012gl050874.

Stammerjohn SE, Maksym T, Heil P, Massom R, Vancoppenolle M, et al. 2011. The influence of winds, sea-surface temperature and precipitation anomalies on Antarctic regional sea-ice conditions during IPY 2007. *Deep-Sea Res Pt II* **58**: 999–1018. doi:10.1016/j.dsr2.2010.10.026.

Stammerjohn SE, Martinson DG, Smith RC, Yuan X, Rind D. 2008. Trends in Antarctic annual sea ice retreat and advance and their relation to ENSO and Southern Annular Mode Variability. *J Geophys Res* **113**: doi:10.1029/2007JC004269.

Steffen K, Key J, Cavalieri DJ, Comiso J, Gloersen P, et al. 1992. The estimation of geophysical parameters using passive microwave algorithms, in Carsey F, ed., *Microwave Remote Sensing of Sea Ice*. Vol. **68**. Washington, D.C.: American Geophysical Union: pp. 201–231.

Steig EJ, Ding Q, Battisti DS, Jenkins A. 2012. Tropical forcing of Circumpolar Deep Water Inflow and outlet glacier thinning in the Amundsen Sea Embayment, West Antarctica. *Ann Glaciol* **53**: 19–28. doi:10.3189/2012AoG60A110.

Swithinbank C. 1988. Satellite image atlas of glaciers of the world: Antarctica. U.S. Geological Survey Professional Paper 1386 B.

Thoma M, Jenkins A, Holland D, Jacobs S. 2008. Modelling Circumpolar Deep Water intrusions on the Amundsen Sea continental shelf, Antarctica. *Geophys Res Lett* **35**: doi:10.1029/2008gl034939.

Toole JM, Krishfield RA, Timmermans M-L, Proshutinsky A. 2011. The Ice-Tethered Profiler: Argo of the Arctic. *Oceanogr* **24**: 126–135. doi:10.5670/oceanog.2011.64.

Turner J, Comiso JC, Marshall G, Lachlan-Cope TA, Bracegirdle T, et al. 2009. Non-annular atmospheric circulation change induced by stratospheric ozone depletion and its role in the recent increase of Antarctic sea ice extent. *Geophys Res Lett* **36**: doi:10.1029/2009GL037524.

Turner J, Phillips T, Hosking JS, Marshall GJ, Orr A. 2013. The Amundsen Sea low. *Int J Climatol* **33**: 1818–1829. doi:10.1002/joc.3558.

van Loon H. 1967. The half-yearly oscillations in middle and high southern latitudes and the coreless winter. *J Atmos Sci* **24**: 472–486.

Wåhlin AK, Muench RD, Arneborg L, Björk G, Ha HK, et al. 2012. Some implications of Ekman layer dynamics for cross-shelf exchange in the Amundsen Sea. *J Phys Oceanogr* **42**: 1461–1474. doi:10.1175/jpo-d-11-041.1.

Walker DP, Jenkins A, Assmann KM, Shoosmith DR, Brandon MA. 2013. Oceanographic observations at the shelf break of the Amundsen Sea, Antarctica. *J Geophys Res-Oceans* **118**: 2906–2918. doi:10.1002/jgrc.20212.

Watkins AB, Simmonds I. 1999. A late spring surge in the open water of the Antarctic sea ice pack. *Geophys Res Lett* **26**: 1481–1484.

Xie H, Tekeli AE, Ackley SF, Yi D, Zwally HJ. 2013. Sea ice thickness estimations from ICESat Altimetry over the Bellingshausen and Amundsen Seas, 2003–2009. *J Geophys Res-Oceans* **118**: 2438–2453. doi:10.1002/jgrc.20179.

Yager P, Sherrell R, Stammerjohn S, Alderkamp A-C, Schofield O, et al. 2012. ASPIRE: The Amundsen Sea Polynya International Research Expedition. *Oceanogr* **25**: 40–53. doi:10.5670/oceanog.2012.73.

Yuan X. 2004. ENSO-related impacts on Antarctic sea ice: a synthesis of phenomenon and mechanisms. *Antarct Sci* **16**: 415–425.

Yuan X, Li C. 2008. Climate modes in southern high latitudes and their impacts on Antarctic sea ice. *J Geophys Res* **113**. doi:10.1029/2006JC004067.

Yuan X, Martinson DG. 2000. Antarctic sea ice extent variability and its global connectivity. *J Climate* **13**: 1697–1717.

Contributions

- Contributed to conception and design: SES
- Contributed to acquisition of data: NASA, NSIDC, ECMWF
- Contributed to analysis and interpretation of data: SES, TM, RAM, KEL, KRA, XY, MR, ER-G, RMS, PLY
- Drafted and/or revised the article: SES, TM, RAM, KEL, KRA, XY, MR, ER-G, RMS, PLY
- Approved the submitted version for publication: SES, TM, RAM, KEL, KRA, XY, MR, ER-G, RMS, PLY

Acknowledgements

The satellite data analyzed here are publicly available from the EOS Distributed Active Archive Center (DAAC) at the National Snow and Ice Data Center, University of Colorado in Boulder, Colorado (nsidc.org). The 10-m wind data were from the European Centre for Medium Range Weather Forecasts (ECMWF) Interim Reanalysis (ERA-I) (www.ecmwf.int). The Envisat image in Figure 1 was provided by the European Space Agency with courtesy and special thanks to Andrew Fleming (British Antarctic Survey) and Polar View (www.polarview.org). Special thanks also go to Leta Schoeller, Michelle LaRue, and Paul Morin at Polar Geospatial Center (www.pgc.umn.edu) for providing ASPIRE with near real-time MODIS Terra images, and to Povl Abrahamsen (British Antarctic Survey) for generating the coastline on Figure 1. Finally, special thanks go to Steve Ackley, two anonymous reviewers, the Editors for their careful and constructive comments on earlier drafts.

Funding information

This project was supported by the National Science Foundation Office of Polar Programs within the division of Antarctic Organisms and Ecosystems (ANT-0838975 to SES/ERG, ANT-0944727 to KRA/KEL, ANT-0838995 to RMS, ANT-0839069 to PLY). For RAM, this work was supported by the Australian Government's Cooperative Research Centre program through the Antarctic Climate and Ecosystems CRC, and contributes to AAS Project 4116. For XY, this work was supported by ANT-0739509.

Competing interests

The authors have declared that no competing interests exist.

Data accessibility statement

The GSFC SMMR-SSM/I sea ice concentration data were from the EOS Distributed Active Archive Center (DAAC) at the National Snow and Ice Data Center, University of Colorado in Boulder, Colorado (http://nsidc.org/data/docs/daac/nsidc0079_bootstrap_seaice.gd.html), and the meteorological reanalysis data are publicly available from the ERA-Interim project (http://www.ecmwf.int/en/research/climate-reanalysis/era-interim). The ITP data of Ackley et al. (2015), mentioned in the Discussion, are available from the Ice-Tethered Profiler Program based at the Woods Hole Oceanographic Institution (http://www.whoi.edu/itp, ITP31; Toole et al., 2011).